IncC plasmid genome rearrangements influence the vertical and horizontal transmission tradeoff in *Escherichia coli*

Margaux Allain[1,2#], Thibaut Morel-Journel[1], Bénédicte Condamine[1], Benoist Gibeaux[2], Benoit Gachet[1], Rémi Gschwind[1], Erick Denamur[1,3], Luce Landraud[1,2]

[1]Université Paris Cité and Université Sorbonne Paris Nord, INSERM, IAME, F-75018 Paris, France.

[2]AP-HP, Laboratoire de Microbiologie Hygiène, Hôpital Louis Mourier, F-92700 Colombes, France.

[3]AP-HP, Laboratoire de Génétique Moléculaire, Hôpital Bichat, F-75018 Paris, France.

[#]Address correspondence to margaux.allain2@aphp.fr, Laboratoire de Microbiologie Hygiène, Hôpital Louis Mourier, 178 rue des Renouillers, 92701 Colombes Cedex, France.

Keywords: IncC plasmid, extended spectrum beta-lactamases, CTX-M, tradeoff, fitness cost

Running Head: IncC plasmid changes and transmission tradeoff

ABSTRACT

Literature has previously described an evolutionary tradeoff between vertical (host growth rate) and horizontal (plasmid conjugation) transmissions, contributing to global plasmid fitness. As conjugative IncC plasmids are especially important for the spread of multidrug resistance (MDR), in an extremely broad range of bacterial hosts, we investigated vertical and horizontal transmissions of two pST3 IncC plasmids according to their backbones and MDR-region rearrangements, upon plasmid entry into a new host. We observed plasmid genome rearrangements after conjugation in three natural *Escherichia coli* clinical strains, varying from null to high number depending on the plasmid, but all occurring in the MDR-region. The plasmid burden on bacterial fitness depended more on the strain background than on the structure of the MDR-region, rearrangements appearing to have no impact. Besides, we observed a statistically significant increase in plasmid transfer rate, from ancestral host to new clinical recipient strains, when the IncC plasmid was rearranged. Finally, we investigated the evolutionary tradeoff of the IncC plasmid during the critical period of plasmid establishment in single K-12 bacterial host, by comparing host bacteria harboring the rearranged or non-rearranged IncC plasmid. Plasmid rearrangements strongly improved conjugation efficiency with no negative growth effect. Our findings indicate that the flexibility of the MDR-region of the IncC plasmids can promote their dissemination, and provide diverse opportunities to capture new resistance genes, especially in an environment subject to selection pressure. In a broader view, they reveal how the vertical-horizontal transmission tradeoff can be manipulated by the plasmid to improve its fitness.

INTRODUCTION

IncC plasmids are large, low copy theta-replicating plasmids, and have an extremely broad-host range. First isolated in the late 1960s, they have been found among agricultural, veterinary, and human clinical isolates worldwide (1–3), including *Aeromonas ssp*, *Yersinia pestis*, *Photobacterium damselae subsp. piscicida*, *Klebsiella pneumoniae*, *Vibrio cholera*, *Escherichia coli*, and *Salmonella enterica* (4).

The term IncA/C has been frequently used to describe plasmids belonging to incompatibility groups A and C (2), linked to some entry-exclusion data which suggested that plasmids from these two groups were very closely related. Two distinct IncA/C lineages, designated A/C_1 and A/C_2, based on the differences in sequence identity of the plasmid amplicons, have been commonly used in the literature to distinguish the IncA plasmid from the IncC group (2, 5). However, recent works of Ambrose *et al.* demonstrated that this designation was incorrect, since IncA and IncC plasmids were in fact compatible (6). Use of these IncA/C terms complicates the description of the phylogeny and evolution of IncC plasmid backbone genes, between the oldest IncC plasmids and contemporary IncC plasmids. It is now well admitted that all IncC plasmids share a highly conserved backbone, and they can be broadly typed into two groups (namely, types 1 and 2), which diverged a long time ago, based on the few differences in their backbones (7). Most of the diversity in IncC plasmid genomes results from changes, confined to three hotspots of integration, consisting of differences within horizontally acquired accessory genes (in particular the gain and deletion of resistance genes) and/or loss of adjacent backbone regions (3, 7–9). Interestingly, some type 1/2-hybrid IncC plasmids have been described, arising from homologous recombination events between the two groups of IncC plasmids, or multi-replicon-hybrid IncC plasmids, resulting from the integration of a plasmid belonging to another incompatibility group into the IncC plasmid genome (9–11).

IncC conjugative plasmids are regarded as a considerable public health threat due to their ability to confer resistance to multiple antimicrobial agents and their contribution to the

dissemination of resistance genes, such as genes encoding AmpC β-lactamases, extended-spectrum β-lactamases (ESBL) or carbapenemases, from long-term hosts to other reservoir bacteria (12–14). The evolution of multidrug resistance (MDR)-encoding modules, via loss and acquisition of diverse islands within two antibiotic resistance islands (designated ARI-A and ARI-B regions) might contribute to the emergence of new antimicrobial resistance in new pathogens.

Although the burden on host cells associated with large costly plasmid acquisition is expected to limit plasmid dissemination in the absence of positive selection, IncC plasmids are frequently described and stably maintained, in an extremely broad range of bacterial hosts. In a previous work, we observed that a costly IncC plasmid was stably maintained without undergoing modification in an *E. coli* laboratory bacterium, while many modifications of the MDR-encoding module appeared immediately after conjugation (15). Two interdependent forces govern the success of multidrug-resistant plasmids: the vertical transmission through cell division and the horizontal transmission through conjugation. In fact, plasmids can exert a variable range of fitness cost on their hosts, resulting in plasmid-carrying cells being outcompeted by plasmid-free cells, with a subsequent impact on the vertical transmission of the plasmid in the absence of positive selection (16). Furthermore, plasmid conjugation constitutes a costly process which may slow host growth rates, in particular immediately after acquisition in a new host (17). Numerous observations in the literature have reported that the plasmid transfer system is often targeted in host-plasmid adaptation processes resulting in decreased conjugation (9, 18, 19). Plasmid costs and conjugation efficiencies depend on general plasmid properties, and an optimal balance between vertical and horizontal transmission modes has been observed to explain high plasmid fitness and prevalence of some plasmids (20).

To gain insights into the role of rearrangements in IncC plasmid fitness, we investigated vertical and horizontal transmission of these plasmids, according to their backbones and MDR-

region rearrangements. More precisely, using an *in vitro* experimental approach and two different ESBL-encoding pST3 IncC plasmids (15), we determined plasmid rearrangement frequency, after conjugation experiments in three clinical *E. coli* recipient strains from the NILS collection (21). We then evaluated the impact of IncC plasmids on bacterial fitness, according to the backbone and MDR-region rearrangements, by determining the plasmid carriage burden on non-rearranged and rearranged plasmid-carrying transconjugants (TCs). We also compared conjugation frequencies to the clinical recipient strains, between plasmids with and without MDR-encoding module rearrangements. Lastly, we performed a second set of conjugation experiments, with *E. coli* K-12 as the recipient host, using the first generation of TCs as donor, to determine the global fitness of IncC plasmid according to the structure of the MDR-encoding region by correlating the plasmid acquisition cost for the K-12 recipient cell and the plasmid transfer rate to that cell (Figure 1).

RESULTS

Rational of the plasmids and strains used for conjugation

To understand the evolutionary mechanisms involved in the dissemination and stability of multidrug-resistant IncC plasmids in bacterial hosts, we used two plasmids (pRCS30 and pRCS46; for simplicity, we will refer to them as p30 and p46, respectively) from a previous collection of sequenced and well-characterized ESBL-encoding plasmids from human clinical *E. coli* strains (CB513 and CB195, respectively) (22). p30 carries a $bla_{\text{CTX-M-14}}$ gene inserted at an ARI-A integration spot, while p46 carries a $bla_{\text{CTX-M-15}}$ gene, and the *IS*Ec9-$bla_{\text{CTX-M-15}}$-*ORF477* transposition unit is inserted in the backbone of the plasmid, between a gene encoding a DNA methylase and a gene encoding a conserved protein of unknown function. Moreover,

p46 has the particularity of being a mosaic plasmid (IncC-IncR plasmid) that has integrated an IncR plasmid within the large MDR-encoding module, inserted at an ARI-A integration spot interrupting *rhs* gene. p46 and p30 are of plasmid multilocus sequence type 3 (pST3) (https://pubmlst.org/plasmid) and belong to the type 2 lineage of IncC plasmids (Figure 2). These two plasmids vary in size from 157 to 246 kb and carry multiple other resistance genes in addition to the $bla_{\text{CTX-M}}$ genes (for additional information, see Materials and Methods, Table S1 and Figure S1**)**. Interestingly, we have observed that a small fraction of the ancestral CB195 donor strain (less than 3% of the total bacterial population) harbored a plasmid, which has spontaneously lost a part of the MDR-encoding module after an *in vitro* experimental evolution (from 80 to 130 generations). Compared to p46, this plasmid (denoted as $p46^{r}$) presents two deletions, a 13,345 bp fragment, just downstream of the *uvrD* gene, encoding the *aacC2-aph-sul2* cassette, which confers resistance to aminoglycosides, and a 48,745 bp fragment encoding the IncR backbone genes and their flanking regions (Table S1 and Figure S1).

We performed multiple independent transfers of these plasmids (p30 from CB513, and p46 and $p46^{r}$ from CB195) in three clinical *E. coli* strains (NILS07, NILS70, and NILS71) made resistant to rifampicin, to obtain multiple independent TCs, denoted as TC-NILS. We selected clinical *E. coli* recipient strains for this study on the basis of their phylogroup, their sequence type representative of the current epidemiology, and their lack of antimicrobial resistance gene (for additional information, see Materials and Methods, Table S1).

Analysis and frequency of plasmid rearrangements in clinical transconjugants

To identify plasmid mutations and rearrangements that may occur after conjugation, we sequenced randomly selected TC-NILS obtained from independent conjugation assays. As no p30 rearrangement was observed in our previous work (15), we sequenced one TC-NILS

obtained after conjugation of p30, and three to six TC-NILS after conjugation of p46, in each clinical recipient strain (n= 20, Table S2).

We used the open-source Breseq pipeline (23) and the ancestral p46 or p30 plasmids as reference genomes. In the first step, we excluded all single nucleotide polymorphisms (SNP), insertions or deletions detected comparing mapping reads of the plasmid references to the assembly of themselves. In the second step, we determined genetic differences occurring between the reference plasmids and the TC-NILS genomes.

For all TC-NILS harboring p30 (denoted as NILS-p30), we observed no plasmid DNA modification after conjugation. In contrast, for 12 of the 14 TC-NILS obtained from p46 plasmid conjugation, we detected rearrangements in the plasmid genome within a large 122,219 bp MDR-region inserted at the integration spot ARI-A (Figure 3 and Table S2). For 10 of these TC-NILS, the rearrangements occurred in two hotspots: an IS*26*-mediated deletion of a sequence encoding the complete backbone of the IncR plasmid and its flanking regions, and an IS*26*-mediated deletion of a sequence carrying aminoglycosides resistance module (*aacC2-aph-sul2* cassette) (Figure 3) (plasmids denoted as $p46^{r}$, TC-NILS denoted as NILS-$p46^{r}$). Four others TC-NILS from conjugation of the p46 plasmid harbored a plasmid without modification of the IncR plasmid genome and of the animoglycosides resistance module (TC513 from NILS70 and TC549 from NILS71), or a plasmid without any rearrangements (TC569 and TC570, both from NILS07) (plasmids denoted as $p46^{nr}$, TC-NILS denoted as NILS-$p46^{nr}$). As expected, we observed a perfect correlation between the presence of antibiotic resistance genes and phenotypic antibiotic sensitivity results (Table S2).

To test whether the high frequency of rearrangement events could be due to a hypermutator profile of the donor strains, we estimated mutation frequencies of strains CB513 (harboring p30) and CB195 (harboring p46) by monitoring their capacity to generate mutations conferring resistance to rifampicin or fosfomycin. We observed no significant differences

compared with the non-hypermutator control strain (Figure S2). Moreover, we detected no mutation in the mismatch repair system in the genome of the strains, suggesting that they were non-hypermutator strains.

To estimate p46 plasmid rearrangement frequency after conjugation in clinical recipient strains, we screened a total of 104 TC-NILS from p46 plasmid conjugation (34, 38, and 32 TCs after conjugation in NILS07, NILS70 and NILS71, respectively), for phenotypic gentamicin resistance and for the presence of the IncR replicase-encoding gene (*repB* gene). Although our method could underestimate the p46 rearrangement frequency, we assumed that it allowed us to determine the minimum rate of plasmid genome modification, in accordance with our previous observations of conjugation-induced p46 rearrangements in these two hotspots. In agreement with the first data, we detected 4 profiles: gentamicin-resistant *repB*-positive strains (with no expected plasmid IncR backbone/aminoglycosides rearrangement), gentamicin-resistant *repB*-negative strains (with deletion of the IncR backbone), *repB*-positive strains with a restoration of gentamicin sensitivity (with deletion of the aminoglycosides cassette), and finally r*epB*-negative and gentamicin-sensitive strains (combining deletion of the IncR backbone and the aminoglycosides cassette). In NILS07, 5.9 % of the TCs had an IncR backbone deletion, 17.6 % of the TCs had their sensitivity to gentamicin restored and 2.9 % of the TCs had both. In NILS70, 10.5 % of the TCs had an IncR deletion, 7.9 % of the TCs had their sensitivity to gentamicin restored and 7.9 % of the TCs had both. In NILS71, 21.9 % of the TCs had an IncR deletion, 9.4 % of the TCs had their sensitivity to gentamicin restored and 6.3 % of the TCs tested had both. (Figure 4).

Overall, the global observed rearrangement rates were high, between 26.3 % (NILS70) and 37.5 % (NILS71), and did not vary according to the recipient strain or the phylogroup (chi-squared test, $P = 0.52$).

Growth burden of IncC plasmids on *E. coli* clinical recipient strains

To evaluate the impact of IncC plasmid carriage on clinical *E. coli* recipient strains, and the growth burden of plasmid rearrangements on the clinical *E. coli* host, we measured maximum growth rates (MGRs) immediately after conjugation. According to the rearrangement profiles and the recipient strains, we tested 14 TC-NILS: 3 NILS-p30, 3 NILS-p46^{nr} without IncR backbone/aminoglycosides rearrangement, and 8 NILS-p46^{r} with IncR backbone/aminoglycosides rearranged plasmid (Table S3). We compared the MGRs of the TC-NILS to the MGRs of the recipient plasmid-free strains (NILS07, NILS70, and NILS71) having been incubated concomitantly with the TC-NILS, and the MGRs of the TC-NILS with each other (Figure 5).

The MGR of TC-NILS were significantly lower than those of the plasmid-free strains, but the difference varied with the strain considered. The greatest decrease was observed in TC-NILS71 (-0.15 div.h^{-1}, $P < 0.0001$), followed by TC-NILS07 (-0.11 div.h^{-1}, $P < 0.0001$) and TC-NILS70 (-0.04 div.h^{-1}, $P = 0.0098$). No significant differences were observed between the MGRs of NILS-p30 and NILS-p46^{nr} ($P = 0.6734$, $P = 0.4674$ and $P = 0.9442$ respectively for the differences between TC-NILS07, TC-NILS70 and TC-NILS71 carrying p30 and those carrying p46^{nr}), or between the MGRs of NILS-p46^{nr} and NILS-p46^{r} ($P = 0.5207$, $P = 0.8884$ and $P = 0.1251$ respectively for the differences between TC-NILS07, TC-NILS70 and TC-NILS71 carrying p46^{nr} and those carrying p46^{r}) (Figure 5).

In conclusion, IncC plasmids systematically entail a cost to bacterial fitness, which varies more depending on the strain background than on MDR-encoding module structure, where rearrangements do not appear to have any impact on growth burden in our model.

Effect of rearrangements on conjugation transfer frequency

To evaluate the impact of rearrangements on horizontal transmission of the p46 plasmid, we used CB195 cells harboring the plasmid which had spontaneously lost part of the MDR-encoding region ($p46^r$) as donor, because the rearrangements were similar to those observed in TC-NILS after conjugation (deletion of the *aacC2-aph-sul2* cassette and the IncR region) (Figure S1), and we compared the transfer rate of p46 and $p46^r$ from the CB195 ancestral strain to the three NILS clinical strains (Figure 6).

In NILS07, the transfer rate of the $p46^r$ plasmid was 10.7 higher than that of the p46 plasmid (4.08×10^{-3} *vs* 3.81×10^{-4}, $P = 0.047$). In NILS70, the transfer rate of the $p46^r$ plasmid was 3.2 higher than that of the p46 plasmid (3.03×10^{-4} *vs* 9.52×10^{-5}, $P = 0.023$). In NILS71, the transfer rate of the $p46^r$ plasmid was 3.4 higher than that of the p46 plasmid (1.30×10^{-4} *vs* 3.86×10^{-5}, $P = 0.028$).

Independently of the background of the recipient strain, we observed a statistically significant increase in the transfer rate of $p46^r$ plasmid compared to p46 plasmid.

Growth-conjugation tradeoff of multidrug-resistant IncC plasmids according to MDR-encoding module rearrangements

The difference in growth dynamics of the clinical recipient strains prevented an accurate estimation of the way IncC plasmid rearrangements affected the vertical and horizontal transmission tradeoff (Figure S3). To overcome this limitation, we modeled plasmid dynamics, using the same *E. coli* K-12 MG1655 host strain and TC-NILS as new plasmid donor strains, enabling general comparison of plasmids excluding confounding host effects. We measured the MGRs of two cell populations (*i.e.* K12 strains harboring $p46^r$ and $p46^{nr}$ plasmids), and determined the $p46^r$ and $p46^{nr}$ transfer rates from TC-NILS donor strains to the K-12 recipient strain.

First, we selected 6 TC-NILS according to their rearrangements and chromosomal backgrounds. Four NILS-p46^{r} presented large rearrangements in the MDR-encoding region (TC574, TC553, TC539 and TC544) (Figure 3) and two NILS-p46^{nr} showed no IncR backbone/aminoglycosides rearrangements (TC570 and TC549) (Table S2). We conducted several independent transfers of each p46^{nr} and p46^{r} plasmid to obtain multiple independent TCs denoted as TC-K12 (referred as TC-K12$_{07}$, TC-K12$_{70}$ and TC-K12$_{71,}$ where the number in subscript refers to the TC-NILS donor strains). After conjugation, we screened the absence of new conjugation-induced IncR backbone/aminoglycosides rearrangements in TC-K12 (for more details, see Table S4).

Second, for each pair TC-NILS donor/K-12 recipient, we measured the MGRs of five randomly selected TC-K12 harboring either p46^{nr} or p46^{r} plasmid (denoted as K12$_{x}$-p46^{nr}, K12$_{x}$-p46^{r-1} or K12$_{x}$-p46^{r-2} according to the observed rearrangement, where the number x in subscript refers to the TC-NILS donor strains) immediately after conjugation. For further analysis, we pooled the MGRs of TC-K12, in respect of the donor strains chromosomal background and p46 plasmid rearrangement, and compared to the MGR of plasmid-free K-12 MG1655. We observed that plasmids imposed a growth burden on the bacterial cell compared to a plasmid-free K-12 MG1655 strain (-0.062 div.h^{-1} for TC-K12$_{07}$, $P < 0.0001$; -0.050 div.h^{-1} for TC-K12$_{70}$, $P < 0.0001$; -0.047 div.h^{-1} for TC-K12$_{71,}$ $P < 0.0001$). The MGRs of TC-K12 strains harboring p46^{r} were either higher than those of TC-K12 strains harboring p46^{nr} (0.026 div.h^{-1} of difference between K12$_{07}$-p46^{nr} and K12$_{07}$-p46^{r-1}, $P = 0.0126$; 0.022 div.h^{-1} of difference between K12$_{71}$-p46^{nr} and K12$_{71}$-p46^{r-2}, $P = 0.0380$) or not significantly different (between K12$_{71}$-p46^{nr} and K12$_{71}$-p46^{r-1}, $P = 0.4886$). Of note, the p46 rearrangement differed between the two p46^{r}-carrying TC-K12$_{71}$, which could explain the variable growth burden of the p46^{r} plasmids on the bacteria host (Figure 7A, for more details, see Table S4).

Third, we compared the transfer rate of $p46^{r}$ and $p46^{nr}$ from TC-NILS to K-12 MG1655 strain. We observed a significantly higher conjugation transfer frequency of the $p46^{r}$ plasmid compared to the $p46^{nr}$ plasmid. The conjugation frequency was 11 times higher from TC-NILS07 carrying $p46^{r}$ than from TC-NILS07 carrying $p46^{nr}$ ($P = 0.0049$) and respectively 155 and 115 times higher from TC-NILS71 $p46^{r}$ with two different rearrangements than from TC-NILS71 carrying $p46^{nr}$ ($P < 0.0001$) (Figure 7B). Interestingly, we observed a significant difference in $p46^{r}$ transfer rates according to the chromosomal background of TC-NILS donor strains (Kruskal-Wallis test, $\chi^2_{df=2} = 7.193$, $P = 0.0274$). Overall, for all clinical strains from which they originated, the $p46^{r}$ transfer rate was higher compared with $p46^{nr}$ plasmids, regardless of their rearrangement, even though the conjugative capacity differed depending on the donor strain (Figure 7B).

Finally, we investigated the relationship between the conjugation frequency and the growth burden of plasmid carriage determined by MGRs measurements for the two cell populations (*i.e.* K12 strains harboring $p46^{r}$ and $p46^{nr}$ plasmids), using the values and confidence intervals of MGR and conjugation frequency fitted by the linear models used for the analysis of these populations. Overall, we observed that the MDR-encoding module rearrangements increased the global fitness of the p46 plasmid, independently of chromosomal background of the donor strain. Indeed, the conjugative capacity of $p46^{r}$ plasmids was systematically higher compared with $p46^{nr}$ plasmids, without increased plasmid-induced growth burden (Figure 8).

DISCUSSION

Understanding the evolutionary mechanisms involved in the success of IncC plasmids is a major challenge, because of their extremely broad host-range, their role in the emergence of resistance to medically important last-resort antimicrobials, and their prevalence in environmental, animal and human bacteria (1, 2, 24). These plasmids share a closely related backbone and have diverged from a common ancestor through the acquisition of integrative elements encoding resistance genes (4, 8, 25). Previous works have suggested that plasmid remodelling occurs during the transfer process (15, 25) without determining the frequency of the phenomena or whether it contributes to beneficial adaptation of the lifecycle's plasmid to different bacterial hosts. Taken together, our observations could explain IncC plasmids frequency among multidrug-resistant clinical bacteria, as these plasmids promote genomic diversity and their own genomic evolution, at a critical stage of their entry into the host cell, with maintenance of global positive fitness.

In this study, we confirmed our previous observation made in a laboratory adapted strain (15), and observed, after plasmid transfer in clinical relevant strains, a variable frequency of rearrangement for type 2 pST3 IncC plasmids, ranging from no event to high rearrangement rates for p30 and p46, respectively. p46 plasmid rearrangements mainly occurred immediately after conjugation and strictly concerned the MDR-encoding module in agreement with previously published observations of plasmid phylogeny (2, 3, 25). Whether the difference in the content of MDR-encoding modules, in ARI-A and ARI-B islands, could alone explain the different rate of plasmid rearrangements observed between p46 and p30 in our model, remains to be determined. Interestingly, p46 contains more integrase genes than p30 and the high density of transposable elements could create recombinational hotspots. The p46 plasmid, as well as the IncA-IncC hybrid plasmid p39R861-4 (26) and many others sequenced IncC plasmids (27), is a mosaic plasmid (IncR-IncC plasmid), which can potentially reveal its high propensity for genomic rearrangements. Conjugative ssDNA transfer can trigger the SOS response and affect

integrase gene expression in integrons, leading to rearrangement of gene cassettes (28). It is well known that the expression of most IncC genes, including large operons involved in the conjugation process (29) as well as the expression of the bet/exo homologous recombination system, depends on a plasmid-borne master activator, AcaCD, which also activates expression of genes carried by distinct families of genomics islands (30–32). Previous studies have shown that conjugative entry of IncC plasmids induced the SOS response in recipient cells and, thought this complex transcriptional regulatory network, served as helper conjugative plasmids to the mobilization and dissemination of genomics islands, via SOS induction (30–32). It is tempting to assume that the SOS response induction in the early timing of broad-host range IncC conjugative plasmid transfer in bacterial host plays a key role in its own genomic organization, constituting an opportune time for extensive DNA exchange and acquisition of new resistance genes, depending on the AcaCD binding sites present in the host cell genome. Our observations highlight the ability of some IncC plasmids to undergo a wide range of genomic modifications, immediately after the conjugation in a new host. With our experimental approach, we deliberately chose all recipient strains without any antibiotic resistance genes, so no acquisition of new antimicrobial genes was observed into IncC plasmids during conjugation. The literature suggests an emergence of IncC plasmids in food animal and human enteric bacteria, originating from an environmental bacterial reservoir (1), and the rapid acquisition of resistance gene modules is associated with antibiotics used in animal agriculture and human therapy. The capture of new antimicrobial genes by IncC plasmids could play a key role as a by-product of rapid adaption of incoming plasmid, in particular in complex bacterial communities with opportunities for co-resident plasmids interactions, in an environment subject to antibiotic selection pressure.

Another important result in our study is the impact of the MDR-encoding module rearrangements of the IncC plasmid, enhancing the fitness of the plasmid in our model. An

evolutionary tradeoff between horizontal and vertical plasmid transmission, a general trait of plasmids, determines plasmid fitness (16). The interdependence between conjugation rate and plasmid growth effect on the bacterial cell is intuitive, and change in the conjugation rate is one of the key processes that reduces the cost of plasmid carriage (18, 33). However, one recent study showed a striking tolerance to increased conjugation efficiencies, across multiple orders of magnitude, without significant growth burden to the host cell for several narrow-host range IncF plasmids (20). In our experiments, conjugation rates were higher for the rearranged IncC plasmids, and plasmid rearrangements did not increase the fitness cost on the recipient strains, during the critical period of plasmid establishment in a new bacterial host. Our observation goes against a systematic conflict between the two modes of plasmid transfer, vertical and horizontal transmission. This ability to improve conjugation efficiency without negative bacterial growth effects could have important implications for IncC plasmids ecology. Despite expected fitness costs, the high flexibility of the MDR-encoding region of the IncC plasmids, generating an increase in their vertical and horizontal plasmid transmission, could promote the dissemination of these plasmids.

Our study has some limitations. First, we used only two types of pST3 IncC plasmids in our model. However, the high structural stability of the genomic backbone of IncC plasmids suggests a direct role for MDR-encoding content in our observation. Further experiments are needed to fully understand the molecular mechanisms underlying genomic changes. Although progress has been made in understanding the molecular biology of broad-host range IncC plasmids, by describing a number of transcriptional regulators, critical to their broad-host dissemination (2, 4), and the high resilience to host defence systems upon entry in a new host by conjugation (34), further investigations are needed to fully understand the molecular mechanisms underlying the ecological success of IncC plasmids. Second, we tested only a small number of clinical host bacteria. However, we chose natural isolates corresponding to

phylogenetically distant isolates with different chromosomal backgrounds, and we obtained the same effect on p46 rearrangements and on the evolution of IncC plasmid fitness. Third, our observations were performed *in vitro* and under a single environmental condition. In previous work, we have shown that p46 can be stably maintained, without undergoing genomic modification, despite having a negative impact on the fitness of the host strain (15). In the present study, we proposed an adaptive process, whereby the vertical and horizontal transmission of p46 improves, and which could allow the maintenance and dissemination of the IncC plasmid in bacterial population. These findings highlight the importance of IncC plasmid as a powerful tool for understanding the evolution of plasmid resistance. Further investigations should be conducted under more complex and relevant conditions, such as microbiome environment.

MATERIALS AND METHODS

Bacterial strains and plasmids

We selected three *E. coli* clinical strains, previously whole-genome sequenced, for this study on the basis of their plasmid replicons and their sequence type (Table S1). They were selected among the Natural Isolates with Low Subcultures (NILS) collection characterized by the absence of *rpoS* mutation (21) and were obtained during January 2013 from two clinical laboratories based in different teaching hospitals in Paris area, France. They were directly sampled from antibiograms on Mueller-Hinton (MH) plates, were sub-cultured only twice and were not subjected to stab storage prior to the extraction of genomic DNA and storage in glycerol at −80°C. NILS07 strain (accession number ERS13474783) of phylogroup A, ST10 according to Achtman multilocus sequence typing (MLST) scheme and serotype O105:H6 was

isolated from feces. NILS70 (accession number ERS13474846), strain of phylogroup B2, ST12 (MLST Achtman scheme) and O4:H5 was isolated from urine. NILS71 (accession number ERS13474847), strain of phylogroup B2, ST1154 (MLST Achtman scheme, single locus variant of ST73) and O2:H1 was isolated from urine. None of these strains carried antimicrobial resistance gene based on whole-genome sequence analysis. We made these three strains resistant to rifampicin (Rif^R) by plating *E. coli* strains incubated in Lysogeny Broth (LB) + 1x Minimum Inhibitory Concentration of rifampicin overnight at 37°C on LB agar medium containing rifampicin (30 mg/L) so that the background remains as close as possible to the original strain. In the end, NILS07 showed a mutation at codon 526 (CAC to CTC), and NILS70 and NILS71 at codon 513 (CAG to CTG) of the *rpoB* gene conferring resistance to rifampicin.

We selected two broad-host range ESBL-encoding pST3 IncC plasmids used in previous studies, pRCS30 (GenBank accession number LT985224) and pRCSC46 (PRJEB70418-ID17151429), which we will referred to as p30 and p46 respectively, for simplicity (15, 22) (Table S1 and Figure S1). p30 (157,836 bp) carries on the one hand a $bla_{\text{CTX-M-14}}$ transposition unit and, on the other hand, a group of four resistance gene (*sul2*, *strA-strB*, *ermMI*, and $bla_{\text{TEM-1}}$) inserted at two different integration spot, named ARI-A and ARI-B by Harmer and Hall (2), respectively. This plasmid originated form an *E. coli* strain of phylogroup F and ST721 (MLST Pasteur scheme) (strain CB513) isolated from a case of bacteriemia in an adult patient in 1999 (Paris area, France). p46 (246,268 bp) carries a $bla_{\text{CTX-M-15}}$ transposition unit which is inserted downstream of a methylase encoding gene. On this plasmid, a large region of 122,219 bp is inserted at the integration spot ARI-A. This region contains two resistance modules (an IS*26*-mediated *aacC2-aph-sul2* cassette followed by a *dfrA-sul1* cassette), a partial IncQ1 replicase and the complete backbone of an IncR plasmid (17,000 bp). The plasmid is thus a composite plasmid, IncC-IncR, which contains two complete replicons. This plasmid originated from an

E. coli strain of phylogroup A and ST718 (MLST Pasteur scheme) (strain CB195) isolated from a case of fecal carriage in an adult patient in 1999 (Paris area, France).

A third plasmid, derived from p46 (denoted as p46^{r}), was obtained in a fraction of the bacterial population of the ancestral strain CB195, after an *in vitro* experimental evolution (80 to 130 generations), and had spontaneously lost the IncR backbone and its flanking regions, as well as the aminoglycosides resistance module (*aacC2-aph-sul2* cassette).

For mutation rate assay, we used *E coli* strain M13, a strong mutator because of a defective mismatch repair system due to MutS inactivation (*mutS* mutant) as a positive control (35), and a wild-type *E. coli* strain K-12 MG1655, as a negative control.

For the conjugation assays with the first transconjugants as donors, we used *E. coli* recipient strain K-12 MG1655 srl::*Tn*10, resistant to tetracyclin.

Mutation rate assay

We estimated mutation frequencies of the isolates by monitoring their capacity to generate mutations conferring resistance to rifampicin or fosfomycin (35). From a glycerol stock, the strains were plated on LB agar and grown overnight at 37°C. We used randomly selected colonies for independent mutation rate assays. They were grown overnight in 10 mL of LB at 37°C under constant stirring at 200 rpm. Next, we transferred 10 µL of the overnight cultures into 990 µL of fresh LB and 100 µL of these cultures were transferred in 10 mL of fresh LB and incubated overnight in the same conditions. Then, we plated appropriate dilutions of the overnight cultures on LB agar without antibiotics, LB agar containing rifampicin (250 mg/L) and LB agar containing fosfomycin (50 mg/L). We counted the rifampin-resistant mutants and fosfomycin-resistant mutants after 24 h at 37°C. We calculated the mutation frequency as the number of mutants obtained on LB with antibiotics divided by the total number

of bacteria on LB without antibiotics. We performed the mutation rate experiments in three biological replicates with at least two technical replicates each.

Conjugation assays

First, we performed independent transfer assays by conjugation of the three ESBL-encoding plasmids (p30, p46, and p46^{r}) from the donors (CB513 and CB195, respectively) to *E. coli* NILS strains (NILS07, NILS70, and NILS71), made resistant to 250 mg/L rifampicin, as the recipient strains. From a glycerol stock, the donor and recipient strains were plated on LB agar and grown overnight at 37°C. We used randomly selected colonies of donor and recipient strains for independent conjugation assays. Donors and recipients were grown overnight in 10 mL of LB at 37°C under constant stirring at 200 rpm. Next, 10 µL of the culture was transferred into 10 mL of fresh LB and incubated for 3 h under the same conditions to obtain an exponential-phase population (OD_{600} = 0.4-0.5). For mating experiments, we mixed 1 mL of culture of the donor strain and 1 mL of culture of the recipient strain (1:1 ratio) and we immediately plated 1.8 mL (9 spots of 200 µL) of mating culture on LB agar without antibiotic at 30°C. After 3 hours of incubation, we resuspended cultures in 5 mL of fresh LB. Then, resuspended mating cultures were plated on LB agar containing rifampicin (250 mg/L) and cefotaxime (4 mg/L) and incubated overnight at 37°C for TCs selection (referred as TC-NILS).

Second, we performed independent transfer assays by conjugation of ESBL-encoding plasmids to *E. coli* recipient strain K-12 MG1655 srl::*Tn*10. For this second conjugation, we selected as donor strains six TC-NILS obtained from our previous conjugation experiments, according to plasmid rearrangements and chromosomal background strain. We used the same protocol as previously, except that we selected the new TCs (referred as TC-K12) using LB agar containing tetracyclin (20 mg/L) and cefotaxime (4 mg/L) (Figure S4).

We calculated the conjugation frequency as the number of TCs divided by the total number of bacteria. We performed the conjugation experiments in three biological replicates with three technical replicates each.

Antimicrobial susceptibility testing

We performed antimicrobial susceptibility testing using the disk diffusion method according to the European Committee on Antimicrobial Susceptibility Testing (EUCAST) guidelines (http://www.eucast.org). The list of antimicrobial compounds that were tested included: ampicillin, amoxicillin-clavulanic acid, ticarcillin, ticarcillin-clavulanic acid, piperacillin, piperacillin-tazobactam, temocillin, cefalexin, cefoxitin, cefixime, ceftazidime, cefotaxime, cefepim, aztreonam, ertapenem, meropenem, imipenem, amikacin, gentamicin, tobramycin, netilmicin, streptomycin, trimethoprim, cotrimoxazole, nalidixic acid, ofloxacin, ciprofloxacin, fosfomycin, tetracycline, rifampicin, chloramphenicol.

Plasmid rearrangement screening

To determine the rearrangement frequencies of the p46 plasmid after conjugation, we screened TCs for phenotypic aminoglycosides resistance (see above for the antimicrobial susceptibility testing), and for the presence of the gene encoding IncR replicase (*repB* gene). We tested TC-NILS obtained from the first conjugation assay between CB195 and NILS strains and TC-K12 obtained from the second conjugation assay between TC-NILS and K-12 MG1655 strain. We obtained the total DNA by boiling lysis method exposing cells to 100°C for 10 min and clarifying the lysate preparations by centrifugation at 15,000 x g for 10 min. We determined the *repB* status on DNA extracts by a specific PCR with a set of primers for IncR-F (5’ TCG CTT CAT TCC TGC TTC AGC 3’) and IncR-R (5’ GTG TGC TGT GGT TAT GCC TCA 3’).

A 251 bp fragment internal to IncR was amplified. We analyzed the amplification products by 1.6 % agarose gel electrophoresis. We also used the PCR-Based Replicon Typing (PBRT) 2.0 Kit (Diatheva, Fano, Italy) to determine replicon content of some TCs, according to the manufacturer's recommendations (36–38).

Whole-genome sequencing

We selected TC-NILS from conjugation of p30 and p46 plasmids for whole-genome sequencing (WGS) using Illumina technology. Briefly, DNA was prepared for indexed, paired-end sequencing on the Illumina MiSeq system (Integragen, MA, USA). DNA samples were extracted using the EZ1 DNA Tissue Kit (Qiagen, Courtaboeuf, France). The DNA was quantified using the Qubit Fluorometer (ThermoFisher Scientific, Asnières sur Seine, France). DNA libraries were prepared and indexed, and tagmentation was processed using the Nextera DNA Flex library Prep kit (Illumina, USA). The sample concentrations were normalized in equimolar concentration at 1 nM. The pooled paired-end libraries were sequenced to a read length of 2 by 300 bp with Illumina MiSeq reagent kit. The genomes were sequenced at an average depth of 50X.

DNA sequence analysis

Illumina genome sequence reads were assessed for quality using FastQC v0.11.8 and subsequently trimmed with a cutoff phred score of 30 using TrimGalore v0.4.5. All genomes were *de novo* assembled using SPAdes v.3.13.1 software and analysed with an in-house bioinformatics pipeline (https://github.com/iame-researchCenter/Petanc) adapted from Bourrel *et al*. (39). Briefly, genome typing was performed including MLST determination, phylogrouping, and serotyping. The pipeline was also used to get information about plasmid

replicons, resistance and virulence genes, the prediction of a plasmid sequence or a chromosome sequence for each contig using PlaScope (40). For each sample, sequenced reads were mapped to a reference sequence to analyze the mutations and rearrangements. For reference chromosomal sequences, we used the NILS sequences extracted *de novo*. For reference plasmid sequences, we used the plasmid sequences annotated on the MicroScope plateform (41). We identified point mutations and rearrangements using the open computational pipeline Breseq v0.27.1 (23). All SNPs identified in the ancestor strains that were sequenced were subtracted from the sequences of the TCs.

Individual bacterial fitness assays

We determined bacterial fitness, defined here as the Maximum Growth Rate (MGR), from growth experiments by OD measurements up to 24 hours of growth. From a glycerol stock, the strains were plated on LB agar and grown overnight at 37°C. We used randomly selected colonies for independent growth assays. They were grown overnight in 10 mL of LB at 37°C under constant stirring at 200 rpm. Next, 200 µL of a 10000-fold dilution of each overnight cultures were incubated in a 96-well flat-bottom microtiter plate (Corning, ME, USA) at 37 °C for 24 hours and were subject to shaking during 60 seconds every two minutes. Optical density (DO 600 nm) was measured automatically every 300 seconds with a microplate reader (Infinite F200-Pro®, Tecan). The measurements were collected using a Python script developed in our laboratory. Each growth curve was characterized by three parameters: the lag time in minute (the time taken to reach the MGR), the MGR in sec^{-1} and the biomass corresponding to the OD_{600} in stationary phase after 24 h of growth. We performed the fitness assays in four biological replicates with three technical replicates each.

Statistical analyses

For the first conjugation assay in NILS strains, the statistical tests were performed with GraphPad Prism version 9.5.1 software. Distribution normality was tested with a Shapiro-Wilk test and either two-tailed unpaired Student t tests or a Mann-Whitney tests were then performed depending on normality. To compare the rearrangements rates, a chi-squared test was used. Differences in MGRs (of TC-NILS and TC-K12) and conjugation frequency in K-12 MG1655 were analyzed using the R software. Linear models were used, with a response variable *Y(x)* (either the MGR of the bacteria or the conjugation frequency of the plasmid from the TC-NILS) computed as a linear combination of coefficients:

$$Y(x) = \beta_0 + \beta_1 I_{x,1} + \beta_2 I_{x,2} + \cdots + \beta_{n-1} I_{n-1,4} + \beta_n I_{x,n} + \epsilon,$$

with ϵ the error, β_0 the intercept, β_i the ith coefficient of the model and $a_{x,i}$ the element of the contrast matrix indicating how coefficient β_i affected the value of *Y(x)* (Table S5).

The contrast matrix characterizing the MGR of TC-NILS was defined such that specific coefficients tested for the difference between given bacteria: β_1 and β_2 characterized differences between TC-NILS07 and respectively TC-NILS70 and TC-NILS71, β_3, β_4 and β_5 characterized differences between bacteria with or without plasmid, respectively among TC-NILS07, TC-NILS70 and TC-NILS71, β_6, β_7 and β_8 characterized differences between p30 and p46^{nr}, respectively among TC-NILS07, TC-NILS70 and TC-NILS71, β_9, β_{10} and β_{11} characterized differences between p46^{nr} and p46^{r}, respectively among TC-NILS07, TC-NILS70 and TC-NILS71.

The contrast matrix characterizing the MGR of TC-K12 was defined such that β_1, β_2 and β_3 characterized the differences between plasmid-free K-12 and respectively TC-K12$_{07}$, TC-K12$_{70}$, TC-K12$_{71}$, β_4 the difference between K12$_{07}$-p46^{nr} and K12$_{07}$-p46^{r-1}, β_5 and β_6 the difference between K12$_{71}$-p46^{nr} and respectively K12$_{71}$-p46^{r-1} and K12$_{71}$-p46^{r-2}.

The contrast matrix characterizing the conjugation frequency was defined such that β_1 and β_2 characterized differences between transfers to TC-K12$_{07}$ and respectively those to TC-K12$_{70}$ and to TC-K12$_{71}$, β_3 characterized the difference between transfers to K12$_{07}$-p46^{nr} and to K12$_{07}$-p46^{r-1}, β_5 and β_6 the difference between transfers to K12$_{71}$-p46^{nr} and respectively to K12$_{71}$-p46^{r-1} and to K12$_{71}$-p46^{r-2}. While values of β_i in the models of MGR correspond to the actual differences in div.h^{-1}, the values of β_i in this model correspond to the log-ratio between the conjugation frequencies.

For all analyses, P values of < 0.05 were considered significant.

ACKNOWLEDGMENTS

We thank Marie-Florence Bredeche for the K-12 MG1655 srl::*Tn*10 strain. We also thank Olivier Clermont, Linda Houhamdi and Marie Petitjean for technical assistance. We are grateful to Olivier Tenaillon for helpful discussion.

This work was partially supported by a grant from the Fondation pour la Recherche Médicale to Erick Denamur (grant number DEQ20161136698). The funders had no role in study design, data collection, and interpretation, or the decision to submit the work for publication.

DATA AVAILABILITY

All reads have been deposited at the European Nucleotide Archive (project accession number PRJEB70418 and PRJEB56162, ID samples from ERS17121429 to ERS17121457, and ERS13474783, ERS13474846 and ERS13474847.

REFERENCES

1. Johnson TJ, Lang KS. 2012. IncA/C plasmids. Mobile Genetic Elements 2:55–58.

2. Harmer CJ, Hall RM. 2015. The A to Z of A/C plasmids. Plasmid 80:63–82.

3. Ambrose SJ, Harmer CJ, Hall RM. 2018. Evolution and typing of IncC plasmids contributing to antibiotic resistance in Gram-negative bacteria. Plasmid 99:40–55.

4. Fernández-Alarcón C, Singer RS, Johnson TJ. 2011. Comparative Genomics of Multidrug Resistance-Encoding IncA/C Plasmids from Commensal and Pathogenic *Escherichia coli* from Multiple Animal Sources. PLOS ONE 6:e23415.

5. Carattoli A, Miriagou V, Bertini A, Loli A, Colinon C, Villa L, Whichard JM, Rossolini GM. 2006. Replicon typing of plasmids encoding resistance to newer beta-lactams. Emerg Infect Dis 12:1145–1148.

6. Ambrose SJ, Harmer CJ, Hall RM. 2018. Compatibility and entry exclusion of IncA and IncC plasmids revisited: IncA and IncC plasmids are compatible. Plasmid 96–97:7–12.

7. Harmer CJ, Hall RM. 2014. pRMH760, a precursor of A/C_2 plasmids carrying bla_{CMY} and bla_{NDM} genes. Microb Drug Resist 20:416–423.

8. Fricke WF, Welch TJ, McDermott PF, Mammel MK, LeClerc JE, White DG, Cebula TA, Ravel J. 2009. Comparative genomics of the IncA/C multidrug resistance plasmid family. J Bacteriol 191:4750–4757.

9. Zhang Y, Lei C-W, Chen X, Yao T-G, Yu J-W, Hu W-L, Mao X, Wang H-N. 2020. Characterization of IncC Plasmids in *Enterobacterales* of Food-Producing Animals Originating From China. Front Microbiol 11:580960.

10. Lei C-W, Kong L-H, Ma S-Z, Liu B-H, Chen Y-P, Zhang A-Y, Wang H-N. 2017. A novel type 1/2 hybrid IncC plasmid carrying fifteen antimicrobial resistance genes recovered from *Proteus mirabilis* in China. Plasmid 93:1–5.

11. Hirabayashi A, Dao TD, Takemura T, Hasebe F, Trang LT, Thanh NH, Tran HH, Shibayama K, Kasuga I, Suzuki M. 2021. A Transferable IncC-IncX3 Hybrid Plasmid Cocarrying $bla_{\text{NDM-4}}$, *tet*(X), and *tmexCD3-toprJ3* Confers Resistance to Carbapenem and Tigecycline. mSphere 6:e0059221.

12. Chihara S, Okuzumi K, Yamamoto Y, Oikawa S, Hishinuma A. 2011. First Case of New Delhi Metallo-β-Lactamase 1–Producing *Escherichia coli* Infection in Japan. Clinical Infectious Diseases 52:153–154.

13. Carattoli A. 2013. Plasmids and the spread of resistance. International Journal of Medical Microbiology 303:298–304.

14. Rozwandowicz M, Brouwer MSM, Fischer J, Wagenaar JA, Gonzalez-Zorn B, Guerra B, Mevius DJ, Hordijk J. 2018. Plasmids carrying antimicrobial resistance genes in *Enterobacteriaceae*. Journal of Antimicrobial Chemotherapy 73:1121–1137.

15. Mahérault A-C, Kemble H, Magnan M, Gachet B, Roche D, Le Nagard H, Tenaillon O, Denamur E, Branger C, Landraud L. 2019. Advantage of the F2:A1:B- IncF Pandemic Plasmid over IncC Plasmids in *In Vitro* Acquisition and Evolution of $bla_{\text{CTX-M}}$ Gene-Bearing Plasmids in *Escherichia coli*. Antimicrob Agents Chemother 63:e01130-19, /aac/63/10/AAC.01130-19.atom.

16. Turner PE, Cooper VS, Lenski RE. 1998. Tradeoff between horizontal and vertical modes of transmission in bacterial plasmids. Evolution 52:315–329.

17. Prensky H, Gomez-Simmonds A, Uhlemann A, Lopatkin AJ. 2021. Conjugation dynamics depend on both the plasmid acquisition cost and the fitness cost. Molecular Systems Biology 17.

18. Zhang J-F, Fang L-X, Chang M-X, Cheng M, Zhang H, Long T-F, Li Q, Lian X, Sun J, Liao X-P, Liu Y-H. 2022. A Trade-Off for Maintenance of Multidrug-Resistant IncHI2 Plasmids in *Salmonella enterica* Serovar Typhimurium through Adaptive Evolution. mSystems 7:e00248-22.

19. San Millan A. 2018. Evolution of Plasmid-Mediated Antibiotic Resistance in the Clinical Context. Trends in Microbiology 26:978–985.

20. Bethke JH, Ma HR, Tsoi R, Cheng L, Xiao M, You L. 2023. Vertical and horizontal gene transfer tradeoffs direct plasmid fitness. Molecular Systems Biology 19: e11300.

21. Bleibtreu A, Clermont O, Darlu P, Glodt J, Branger C, Picard B, Denamur E. 2014. The *rpoS* gene is predominantly inactivated during laboratory storage and undergoes source-sink evolution in *Escherichia coli* species. J Bacteriol 196:4276–4284.

22. Branger C, Ledda A, Billard-Pomares T, Doublet B, Fouteau S, Barbe V, Roche D, Cruveiller S, Médigue C, Castellanos M, Decré D, Drieux-Rouze L, Clermont O, Glodt J, Tenaillon O, Cloeckaert A, Arlet G, Denamur E. 2018. Extended-spectrum β-lactamase-encoding genes are spreading on a wide range of *Escherichia coli* plasmids existing prior to the use of third-generation cephalosporins. Microbial Genomics 4.

23. Deatherage DE, Barrick JE. 2014. Identification of mutations in laboratory-evolved microbes from next-generation sequencing data using breseq. Methods Mol Biol 1151:165–188.

24. Doublet B, Boyd D, Douard G, Praud K, Cloeckaert A, Mulvey MR. 2012. Complete nucleotide sequence of the multidrug resistance IncA/C plasmid pR55 from *Klebsiella pneumoniae* isolated in 1969. Journal of Antimicrobial Chemotherapy 67:2354–2360.

25. Meinersmann RJ, Lindsey RL, Bono JL, Smith TP, Oakley BB. 2013. Proposed model for the high rate of rearrangement and rapid migration observed in some IncA/C plasmid lineages. Appl Environ Microbiol 79:4806–4814.

26. Anantham S, Harmer CJ, Hall RM. 2015. p39R861-4, A Type 2 A/C2 Plasmid Carrying a Segment from the A/C1 Plasmid RA1. Microb Drug Resist 21:571–576.

27. Pesesky MW, Tilley R, Beck DAC. 2019. Mosaic plasmids are abundant and unevenly distributed across prokaryotic taxa. Plasmid 102:10–18.

28. Baharoglu Z, Bikard D, Mazel D. 2010. Conjugative DNA Transfer Induces the Bacterial SOS Response and Promotes Antibiotic Resistance Development through Integron Activation. PLOS Genetics 6:e1001165.

29. Hancock SJ, Phan M-D, Luo Z, Lo AW, Peters KM, Nhu NTK, Forde BM, Whitfield J, Yang J, Strugnell RA, Paterson DL, Walsh TR, Kobe B, Beatson SA, Schembri MA. 2020. Comprehensive analysis of IncC plasmid conjugation identifies a crucial role for the transcriptional regulator AcaB. Nat Microbiol 5:1340–1348.

30. Douard G, Praud K, Cloeckaert A, Doublet B. 2010. The *Salmonella* Genomic Island 1 Is Specifically Mobilized In Trans by the IncA/C Multidrug Resistance Plasmid Family. PLoS ONE 5:e15302.

31. Carraro N, Matteau D, Burrus V, Rodrigue S. 2015. Unraveling the regulatory network of IncA/C plasmid mobilization: When genomic islands hijack conjugative elements. Mob Genet Elements 5:1–5.

32. Pons MC, Praud K, Da Re S, Cloeckaert A, Doublet B. 2023. Conjugative IncC Plasmid Entry Triggers the SOS Response and Promotes Effective Transfer of the Integrative Antibiotic Resistance Element SGI1. Microbiol Spectr 11:e02201-22.

33. San Millan A, MacLean RC. 2017. Fitness Costs of Plasmids: a Limit to Plasmid Transmission. Microbiol Spectr 5:5.5.02.

34. Roy D, Huguet KT, Grenier F, Burrus V. 2020. IncC conjugative plasmids and SXT/R391 elements repair double-strand breaks caused by CRISPR-Cas during conjugation. Nucleic Acids Res 48:8815–8827.

35. Picard B, Duriez P, Gouriou S, Matic I, Denamur E, Taddei F. 2001. Mutator Natural *Escherichia coli* Isolates Have an Unusual Virulence Phenotype. Infect Immun 69:9–14.

36. Carloni E, Andreoni F, Omiccioli E, Villa L, Magnani M, Carattoli A. 2017. Comparative analysis of the standard PCR-Based Replicon Typing (PBRT) with the commercial PBRT-KIT. Plasmid 90:10–14.

37. Carattoli A, Bertini A, Villa L, Falbo V, Hopkins KL, Threlfall EJ. 2005. Identification of plasmids by PCR-based replicon typing. J Microbiol Methods 63:219–228.

38. Carattoli A. 2009. Resistance plasmid families in *Enterobacteriaceae*. Antimicrob Agents Chemother 53:2227–2238.

39. Bourrel AS, Poirel L, Royer G, Darty M, Vuillemin X, Kieffer N, Clermont O, Denamur E, Nordmann P, Decousser J-W, IAME Resistance Group, Lafaurie M, Bercot B, Walewski V, Lescat M, Carbonnelle E, Ousser F, Idri N, Ricard J-D, Landraud L, Le Dorze M, Jacquier H, Cambau E, Lepeule R, Gomart C. 2019. Colistin resistance in Parisian inpatient faecal *Escherichia coli* as the result of two distinct evolutionary pathways. Journal of Antimicrobial Chemotherapy 74:1521–1530.

40. Royer G, Decousser JW, Branger C, Dubois M, Médigue C, Denamur E, Vallenet D. 2018. PlaScope: a targeted approach to assess the plasmidome from genome assemblies at the species level. Microbial Genomics 4.

41. Médigue C, Calteau A, Cruveiller S, Gachet M, Gautreau G, Josso A, Lajus A, Langlois J, Pereira H, Planel R, Roche D, Rollin J, Rouy Z, Vallenet D. 2017. MicroScope-an integrated resource for community expertise of gene functions and comparative analysis of microbial genomic and metabolic data. Brief Bioinformatics https://doi.org/10.1093/bib/bbx113.

FIG 1: Workflow overview. First, multiple independent transfers of two plasmids (p30 and p46 from CB513 and CB195 wild type (WT) donor strains, respectively) in 3 clinical *E. coli* recipient strains (NILS07, NILS70, and NILS71; made resistant to rifampicin (Rif^R)) were performed to obtain multiple NILS transconjugants (denoted as TC-NILS). $^{\$}$, Independent transfers of p46 plasmid, which spontaneously exhibited rearrangements into the MDR-encoding region and selected from the ancestral donor strain CB195 (designated $p46^r$), were also performed in the 3 *E. coli* NILS recipient strains. Second, conjugation between previously formed TC-NILS (harboring $p46^r$ or non-rearranged p46 plasmid, designated $p46^{nr}$) and K-12 MG1655 were performed to obtain multiple K-12 transconjugants (denoted as TC-K12). Rearrangements that occurred during conjugation were analyzed by whole-genome sequencing and their frequency was evaluated. Growth rates of the transconjugants were measured and the transfer rates of the various plasmids were determined. Finally, statistical modelling was used to determine the impact of rearrangements on vertical and horizontal plasmid transmission tradeoff.

FIG 2: Comparative map of p30 (157,836 bp, type 2 IncC plasmid) and p46 (246,268 bp, type 2 IncC-IncR plasmid) plasmids, with plasmid pRMH760 (170,613 bp, type 1a IncC plasmid, GenBank accession number KF976462) used as reference, generated using Blast Ring Image Generator (BRIG) diagram. The outer circle (green) represent the genome of the p46 plasmid, the central circle (blue) represent the genome of the p30 plasmid and the inner circle (gray) represent the genome of the reference plasmid pRMH760. Open reading frames are shown as arrow indicating the direction of transcription. The ARI-A (MDR-encoding region) and ARI-B islands are indicated by double arrows.

FIG 3: Rearrangements detected in the p46 plasmid genome after conjugation of donor strain CB195 in 3 *E. coli* clinical isolates (NILS07, NILS70, and NILS71; indicated on the left). The linear map of the plasmid is presented and open reading frames are shown as arrows indicating the direction of transcription (dark blue, plasmid transfer; yellow, replication; light blue, plasmid maintenance; red, resistance; black, metabolism; pink, mobile elements and white, hypothetical proteins). The IncR plasmid is indicated by dotted line. The MDR-encoding region inserted at the integration spot ARI-A is indicated by double arrow. For rearrangements, the deletions observed in each transconjugant (TC-NILS) are indicated by gray boxes. Green triangles indicate the areas targeted in the rearrangement screening (see text). Asterisks indicate TC-NILS used in conjugation experiments in *E. coli* K-12 MG1655 (see text).

FIG 4: Share of isolates presenting plasmid IncR backbone/aminoglycosides rearrangements after conjugation of the donor strain CB195 in 3 *E. coli* clinical strains (NILS07, NILS70, and NILS71)

FIG 5: Scatter plot representation of the maximum growth rates (MGRs) of each NILS and TC-NILS. For each NILS, MGRs of NILS-Rif^{R} with no plasmid (empty circle), NILS-p30 (full circle), NILS-p46^{nr} (full circle), and NILS-p46^{r} (circle-cross) are represented. **(A)**, MGRs of plasmid-free and plasmid-carrying NILS07. **(B)**, MGRs of plasmid-free and plasmid-carrying NILS70. **(C)**, MGRs of plasmid-free and plasmid-carrying NILS71. Each dot represents the result of one experiment. Each central line represents the mean of all the experiments. All experiments were performed in three technical replicates. Asterisks indicate significant differences (**, $P \leq 0.01$; ****, $P \leq 0.0001$); ns, not significant.

FIG 6: Scatter plot representation of the transfer frequency observed after conjugation of p46 (full circle) and p46^{r} (circle-cross), from ancestral donor strain CB195 to *E. coli* NILS strains. The dotted lines separate the different NILS strains. Each dot represents the result of one conjugation experiment. Each central line represents the mean of all the experiments. All experiments were performed in three biological replicates, with three technical replicates each. Asterisks indicate significant differences (*, $P \leq 0.05$; **, $P \leq 0.01$). $^{\$}$ Here, p46^{r} plasmid was obtained from the ancestral donor strain CB195, and spontaneously exhibited rearrangements in the MDR-encoding region.

FIG 7: (A), Scatter plot representation of the maximum growth rates (MGRs) of K-12 and TC-K12, obtained after conjugation of p46^{nr} (full circle) and p46^{r} (circle-cross) from TC-NILS to *E. coli* K-12 MG1655 srl::*Tn*10 strain. The dotted lines separate the TC-K12 according to the chromosomal background of TC-NILS donor strains. Each dot represents the result of one experiment. Each central line represents the mean of all the experiments. All experiments were performed in three technical replicates. Asterisks indicate significant differences (*, $P \leq 0.05$;

****, $P \leq 0.0001$), ns, not significant. **(B),** Scatter plot representation of the conjugation frequency of p46^{nr} (full circle) and p46^{r} (circle-cross) from TC-NILS to *E. coli* K-12 MG1655 srl::*Tn*10 strain. The dotted lines separate the TC-NILS donor strains according to their chromosomal background (*i.e.* NILS strains). Each dot represents the result of one conjugation experiment. Each central line represents the mean of all the experiments. All experiments were performed in three biological replicates, with three technical replicates each. Asterisks indicate significant differences (**, $P \leq 0.01$; ****, $P \leq 0.0001$), ns, not significant.

FIG 8: Two-dimensional representation of p46 plasmid dynamics. Relationship between the conjugation frequencies (x-axis) of p46^{nr} (full circle) or p46^{r} (circle-cross) from TC-NILS donor strains to K-12 MG1655 recipient strain, and maximum growth rates (MGRs) (y-axis) of the TC-K12 transconjugants obtained. All MGRs experiments were performed in five biological replicates, with three technical replicates, and all conjugation experiments were performed in three biological replicates, with three technical replicates each. The dotted line (which passes through the highest fitness value obtained in p46^{nr} plasmids and the lowest fitness value obtained in p46^{r} plasmids) separates their relative global fitness (low *vs* high).

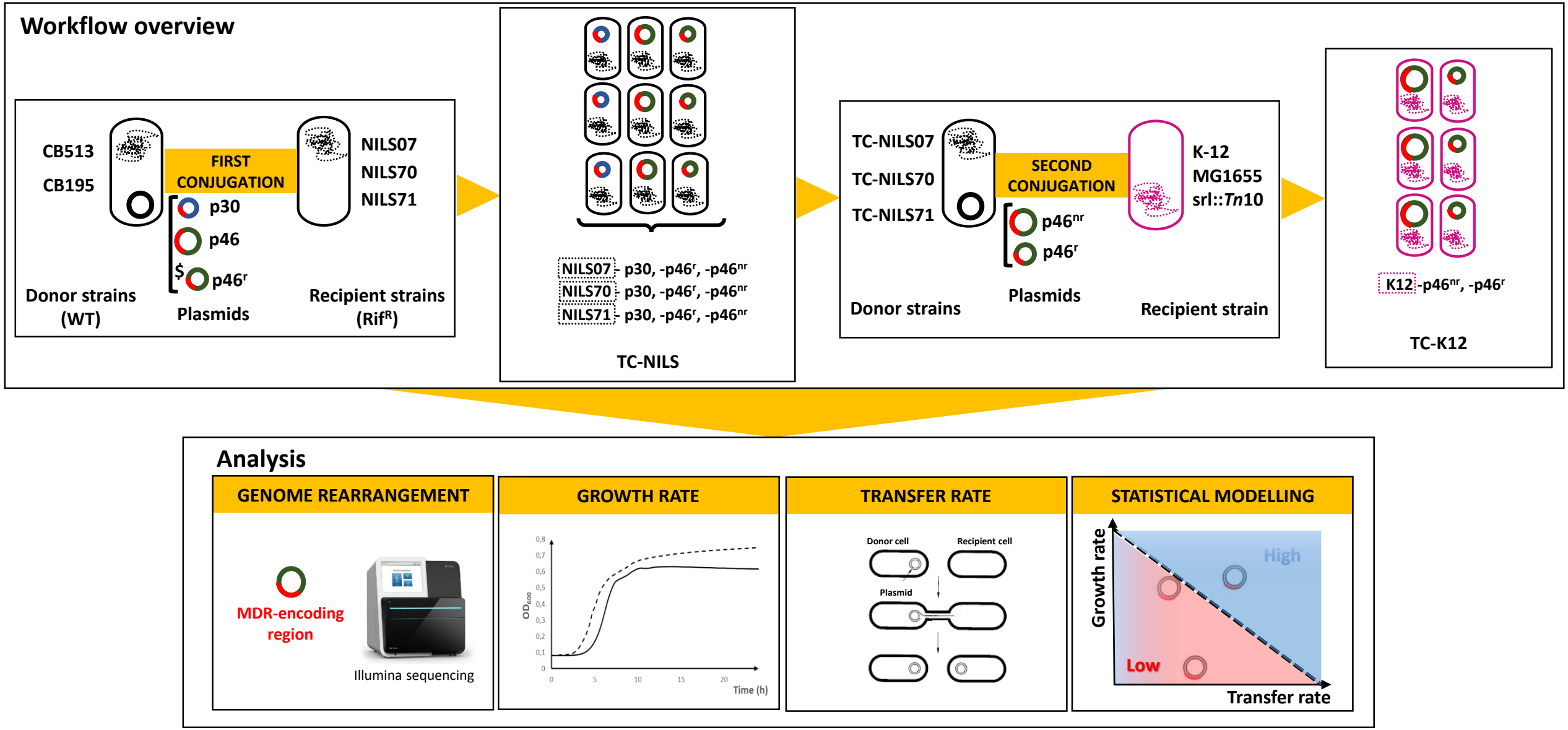

FIG 1: Workflow overview. First, multiple independent transfers of two plasmids (p30 and p46 from CB513 and CB195 wild type (WT) donor strains, respectively) in 3 clinical *E. coli* recipient strains (NILS07, NILS70, and NILS71; made resistant to rifampicin (Rif^R)) were performed to obtain multiple NILS transconjugants (denoted as TC-NILS). $^{\$}$, Independent transfers of p46 plasmid, which spontaneously exhibited rearrangements into the MDR-encoding region and selected from the ancestral donor strain CB195 (designated $p46^r$), were also performed in the 3 *E. coli* NILS recipient strains. Second, conjugation between previously formed TC-NILS (harboring $p46^r$ or non-rearranged p46 plasmid, designated $p46^{nr}$) and K-12 MG1655 were performed to obtain multiple K-12 transconjugants (denoted as TC-K12). Rearrangements that occurred during conjugation were analyzed by whole genome sequencing and their frequency was evaluated. Growth rates of the transconjugants were measured and the transfer rates of the various plasmids were determined. Finally, statistical modelling was used to determine the impact of rearrangements on vertical and horizontal plasmid transmission tradeoff.

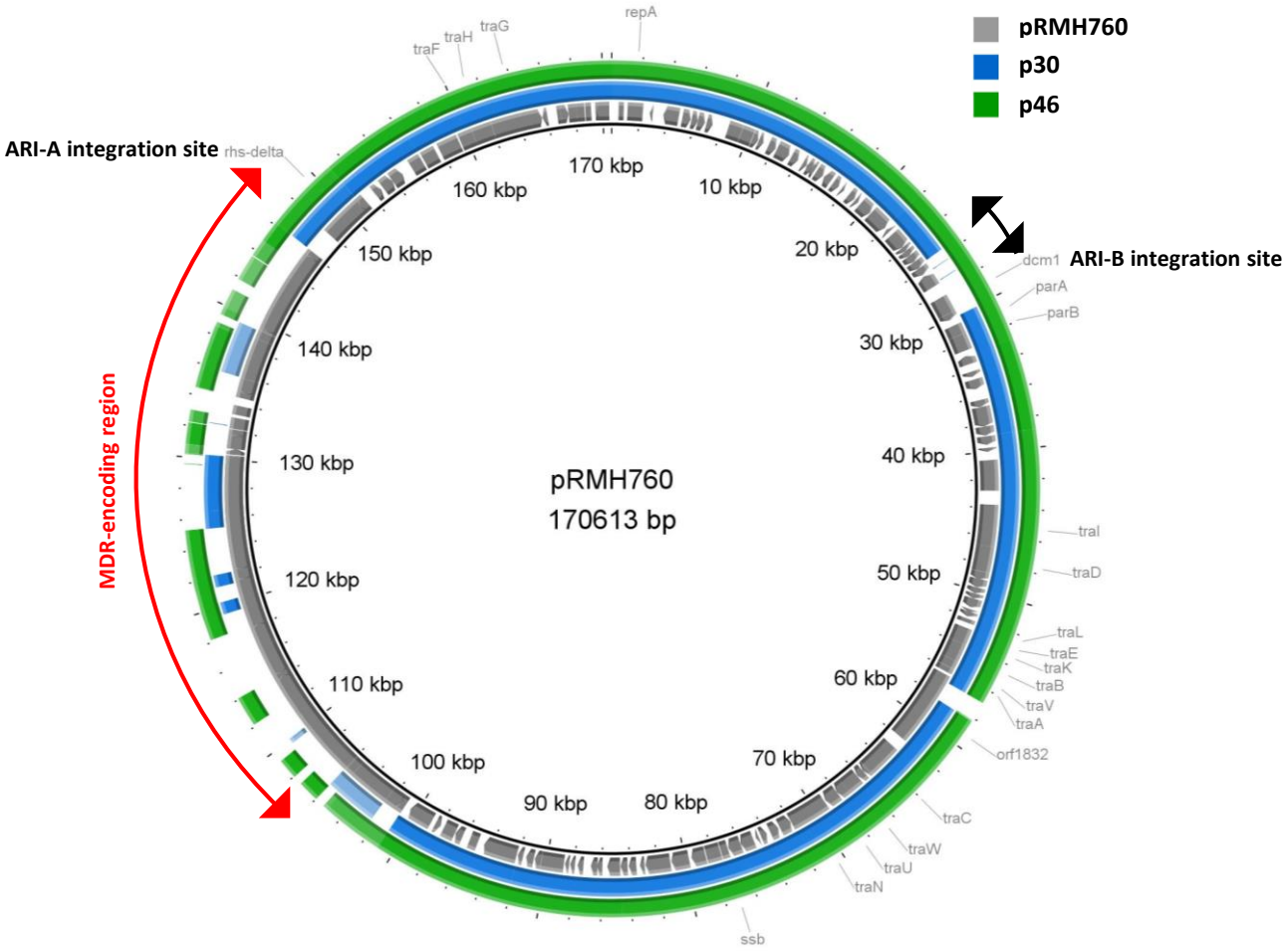

FIG 2: Comparative map of p30 (157,836 bp, type 2 IncC plasmid) and p46 (246,268 bp, type 2 IncC-IncR plasmid) plasmids, with plasmid pRMH760 (170,613 bp, type 1a IncC plasmid, GenBank accession number KF976462) used as reference, generated using Blast Ring Image Generator (BRIG) diagram. The outer circle (green) represent the genome of the p46 plasmid, the central circle (blue) represent the genome of the p30 plasmid and the inner circle (gray) represent the genome of the reference plasmid pRMH760. Open reading frames are shown as arrow indicating the direction of transcription. The ARI-A (MDR-encoding region) and ARI-B islands are indicated by double arrows.

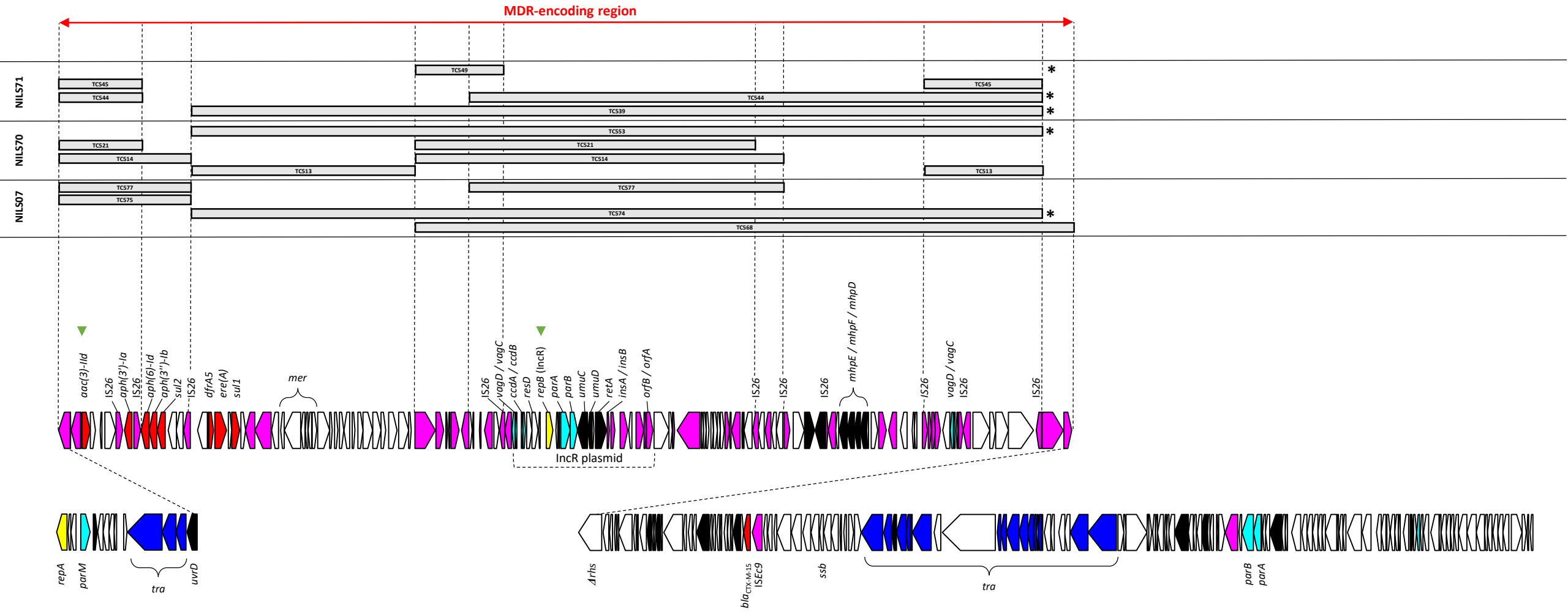

FIG 3: Rearrangements detected in the p46 plasmid genome after conjugation of donor strain CB195 in 3 *E. coli* clinical isolates (NILS07, NILS70, and NILS71; indicated on the left). The linear map of the plasmid is presented and open reading frames are shown as arrows indicating the direction of transcription (dark blue, plasmid transfer; yellow, replication; light blue, plasmid maintenance; red, resistance; black, metabolism; pink, mobile elements and white, hypothetical proteins). The IncR plasmid is indicated by dotted line. The MDR-encoding region inserted at the integration spot ARI-A is indicated by double arrow. For rearrangements, the deletions observed in each transconjugant (TC-NILS) are indicated by gray boxes. Green triangles indicate the areas targeted in the rearrangement screening (see text). Asterisks indicate TC-NILS used in conjugation experiments in *E. coli* K-12 MG1655 (see text).

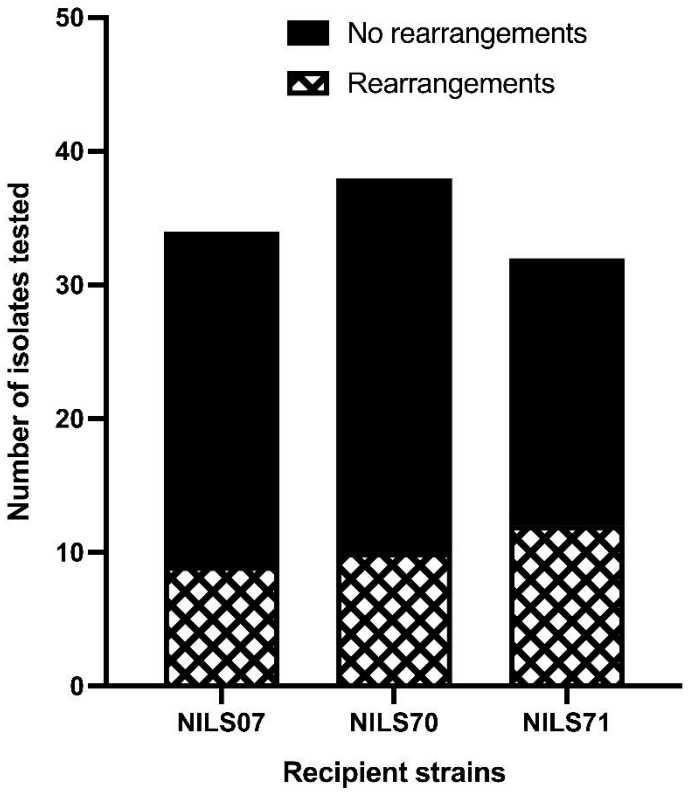

FIG 4 : Share of isolates presenting plasmid IncR backbone/aminoglycosides rearrangements after conjugation of the donor strain CB195 in 3 *E. coli* clinical strains (NILS07, NILS70, and NILS71)

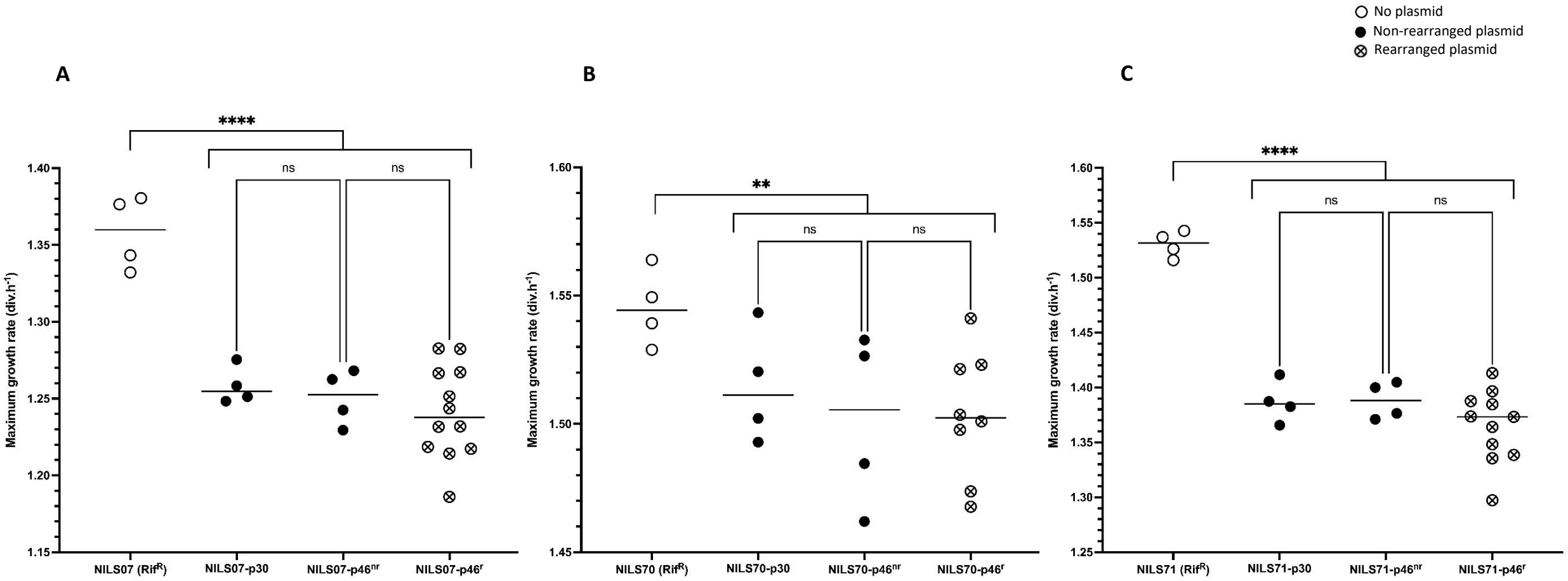

FIG 5: Scatter plot representation of the maximum growth rates (MGRs) of each NILS and TC-NILS. For each NILS, MGRs of NILS-Rif^{R} with no plasmid (empty circle), NILS-p30 (full circle), NILS-p46^{nr} (full circle), and NILS-p46^{r} (circle-cross) are represented. (A) MGRs of plasmid-free and plasmid-carrying NILS07. (B) MGRs of plasmid-free and plasmid-carrying NILS70. (C) MGRs of plasmid-free and plasmid-carrying NILS71. Each dot represents the result of one experiment. Each central line represents the mean of all the experiments. All experiments were performed in three technical replicates. Asterisks indicate significant differences (**, $P \leq 0.01$; ****, $P \leq 0.0001$); ns, not significant.

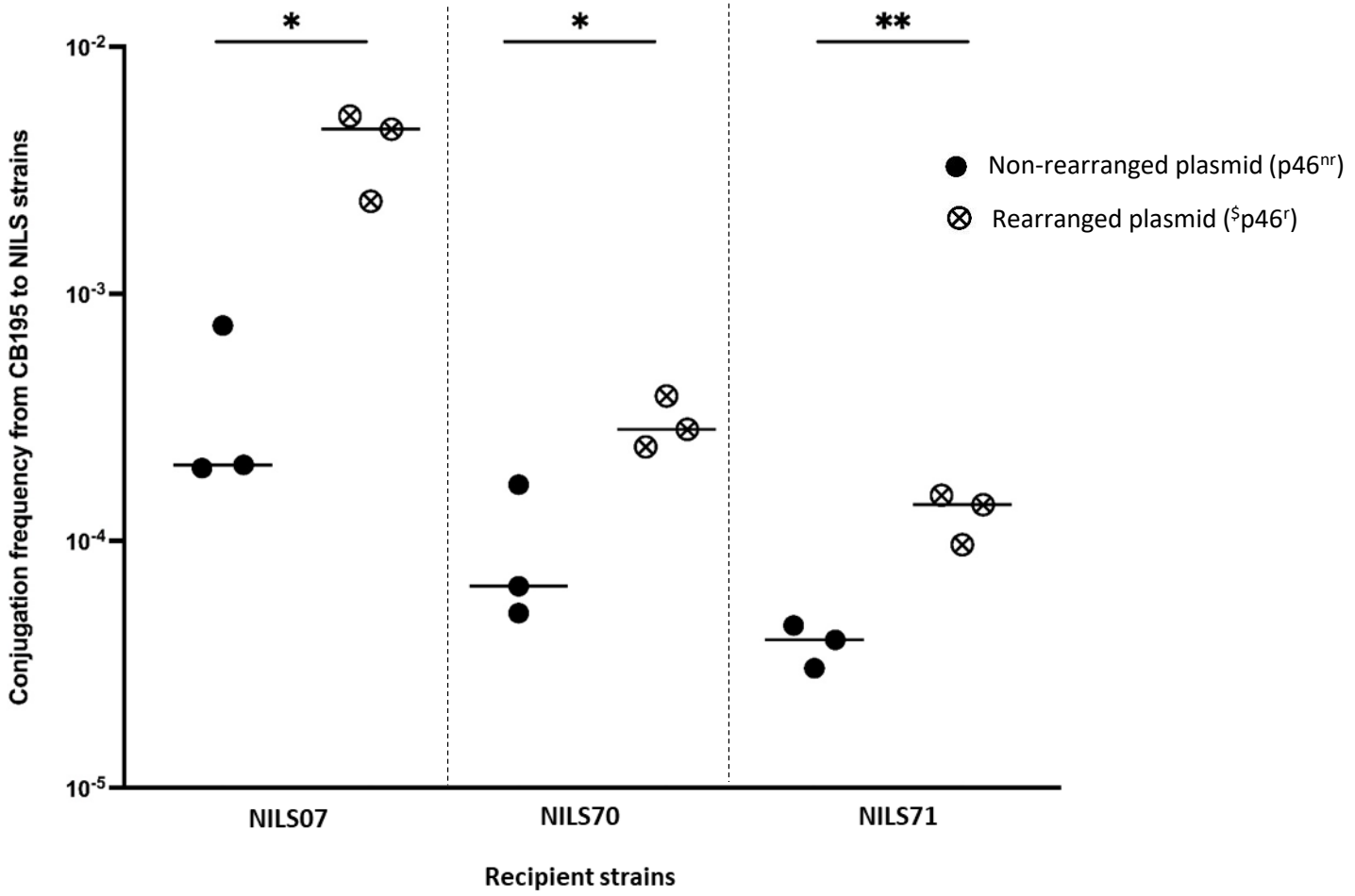

FIG 6: Scatter plot representation of the transfer frequency observed after conjugation of p46 (full circle) and p46^{r} (circle-cross), from ancestral donor strain CB195 to *E. coli* NILS strains. The dotted lines separate the different NILS strains. Each dot represents the result of one conjugation experiment. Each central line represents the mean of all the experiments. All experiments were performed in three biological replicates, with three technical replicates each. Asterisks indicate significant differences (*, $P \leq 0{,}05$ **, $P \leq 0{,}01$). $^{\$}$Here, p46^{r} plasmid was obtained from the ancestral donor strain CB195, and spontaneously exhibited rearrangements in the MDR-encoding region.

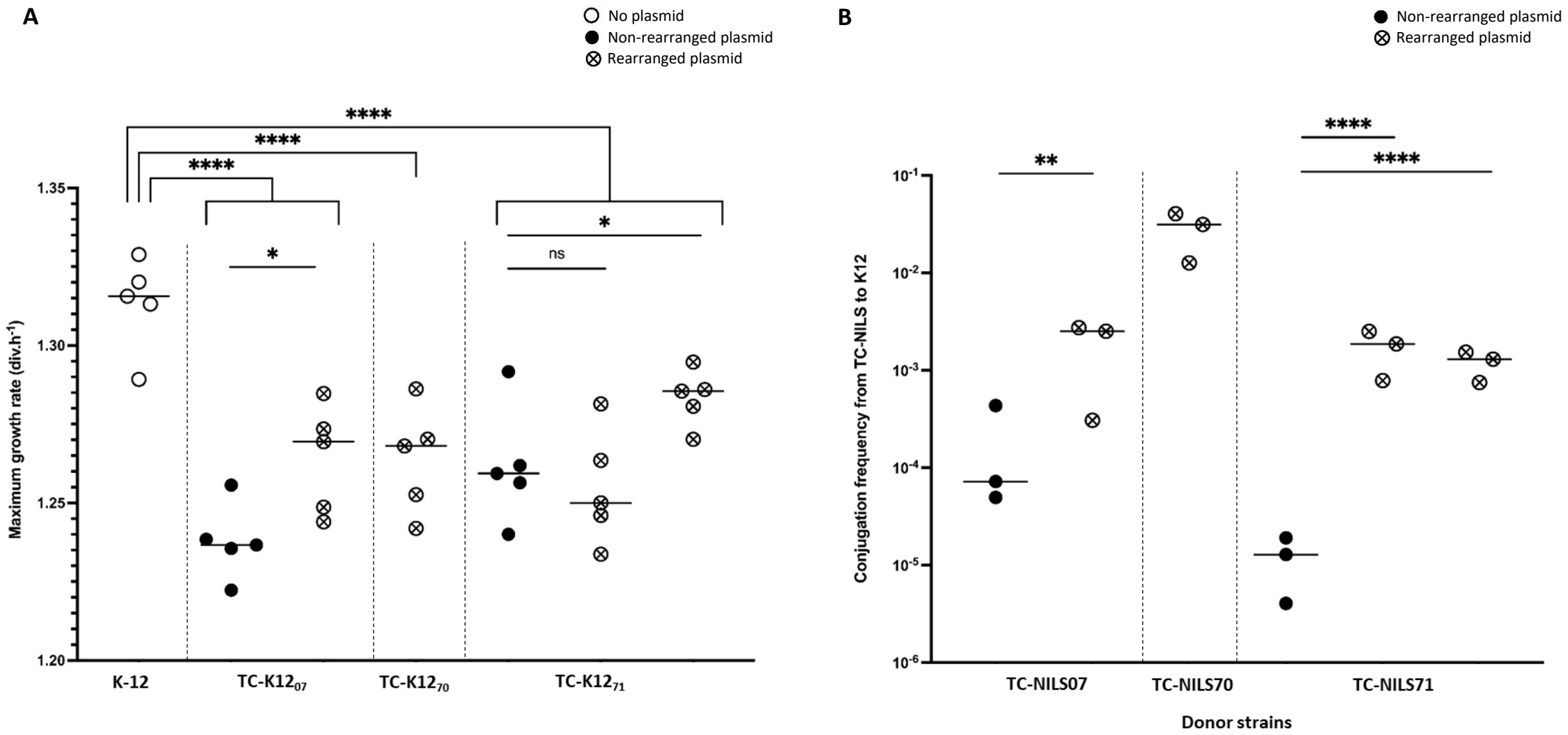

FIG 7: (A) Scatter plot representation of the maximum growth rates (MGRs) of K-12 and TC-K12, obtained after conjugation of p46^{nr} (full circle) and p46^{r} (circle-cross) from TC-NILS to *E. coli* K-12 MG1655 srl::*Tn*10 strain. The dotted lines separate the TC-K12 according to the chromosomal background of TC-NILS donor strains. Each dot represents the result of one experiment. Each central line represents the mean of all the experiments. All experiments were performed in three technical replicates. Asterisks indicate significant differences (*, $P \leq 0.05$; ****, $P \leq 0.0001$), ns, not significant. . (B) Scatter plot representation of the conjugation frequency of p46^{nr} (full circle) and p46^{r} (circle-cross) from TC-NILS to *E. coli* K-12 MG1655 srl::*Tn*10 strain. The dotted lines separate the TC-NILS donor strains according to their chromosomal background (*i.e.* NILS strains). Each dot represents the result of one conjugation experiment. Each central line represents the mean of all the experiments. All experiments were performed in three biological replicates, with three technical replicates each. Asterisks indicate significant differences (**, $P \leq 0.01$; ****, $P \leq 0.0001$), ns, not significant.

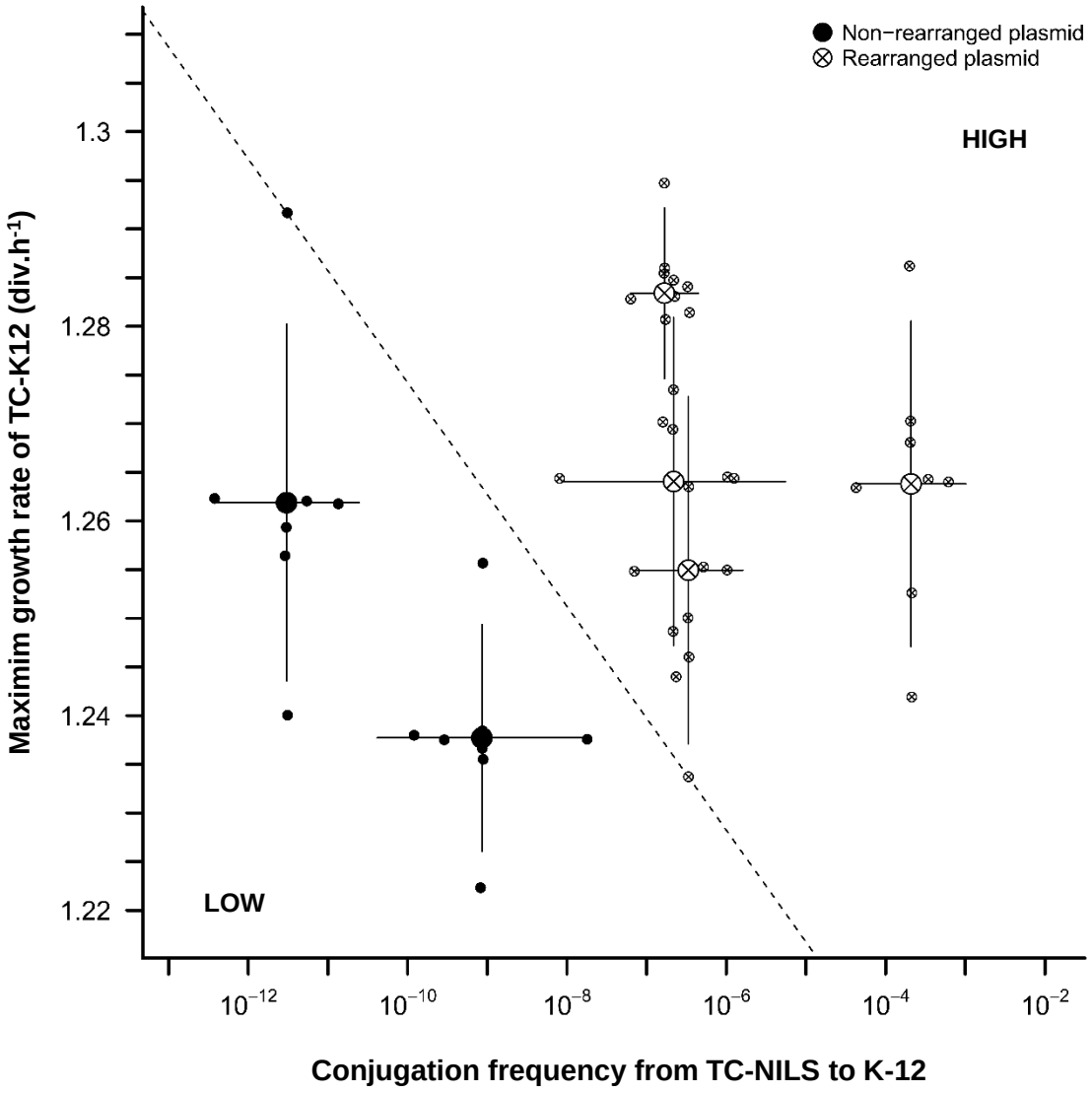

FIG 8: Two-dimensional representation of p46 plasmid dynamics. Relationship between the conjugation frequencies (x-axis) of p46^{nr} (full circle) or p46^{r} (circle-cross) from TC-NILS donor strains to K-12 MG1655 recipient strain, and maximum growth rates (MGRs) (y-axis) of the TC-K12 transconjugants obtained. All MGRs experiments were performed in five biological replicates, with three technical replicates, and all conjugation experiments were performed in three biological replicates, with three technical replicates each. The dotted line (which passes through the highest fitness value obtained in p46^{nr} plasmids and the lowest fitness value obtained in p46^{r} plasmids) separates their relative global fitness (low *vs* high).

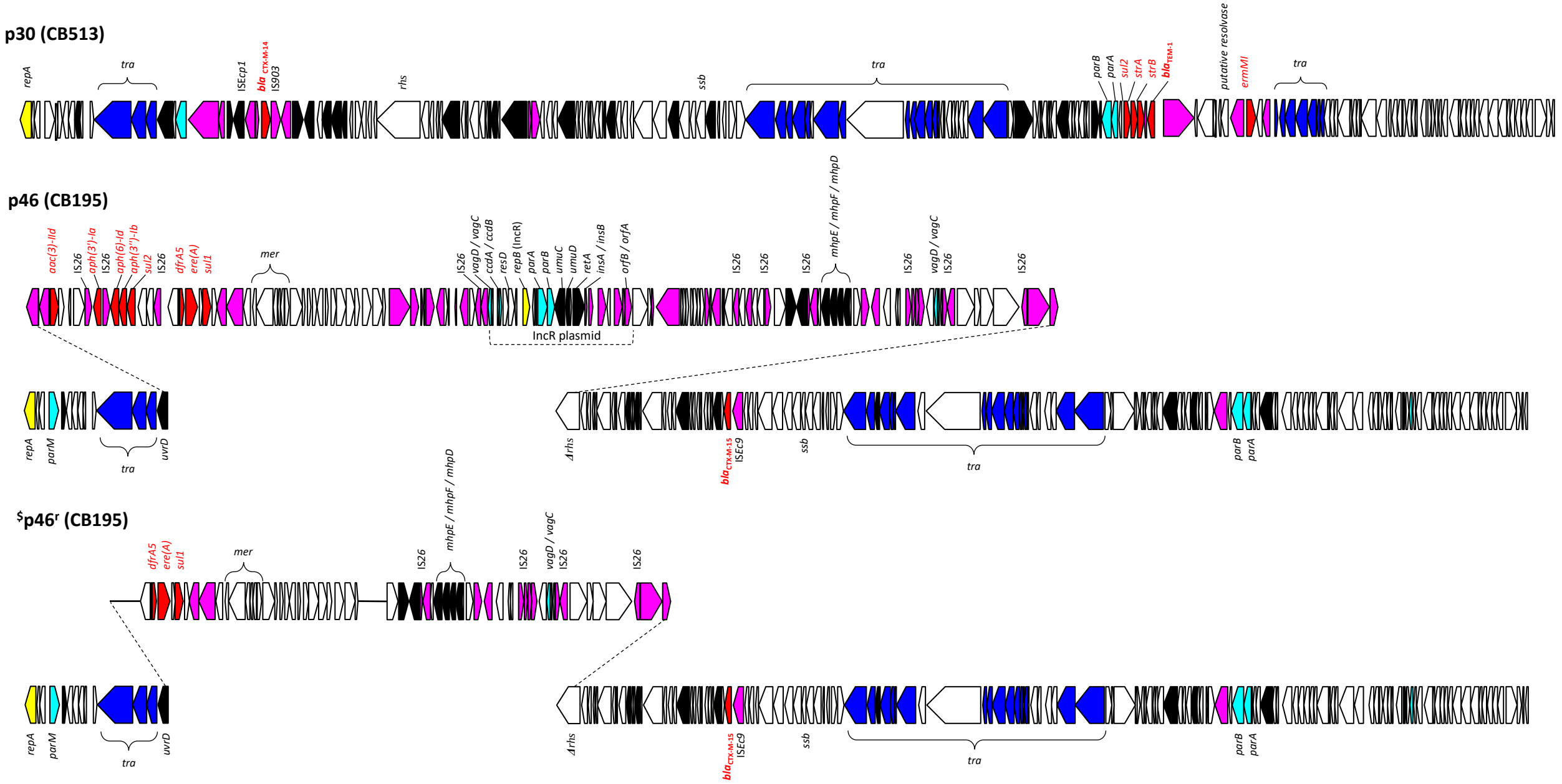

FIG S1: Linear maps of p30 (IncC, pST3, from CB513) and p46 (IncC-IncR, pST3, from CB195) ancestral plasmids. Open reading frames are shown as arrows indicating the direction of transcription. Dark blue, plasmid transfer; yellow, replication; light blue, plasmid maintenance; red, resistance; black, metabolism; pink, mobile elements and white, hypothetical proteins. $ Rearranged p46 (denoted as p46^{r}) plasmid (IncC, pST3), from CB195 ancestral donor strain and which spontaneously exhibited rearrangements into the MDR-encoding region, is also represented. Deleted regions in p46^{r} compared to p46 (IncR backbone genes and their flanking regions including the *aacC2-aph-sul2* cassette which confers resistance to aminoglycosides) are represented by a solid black line.

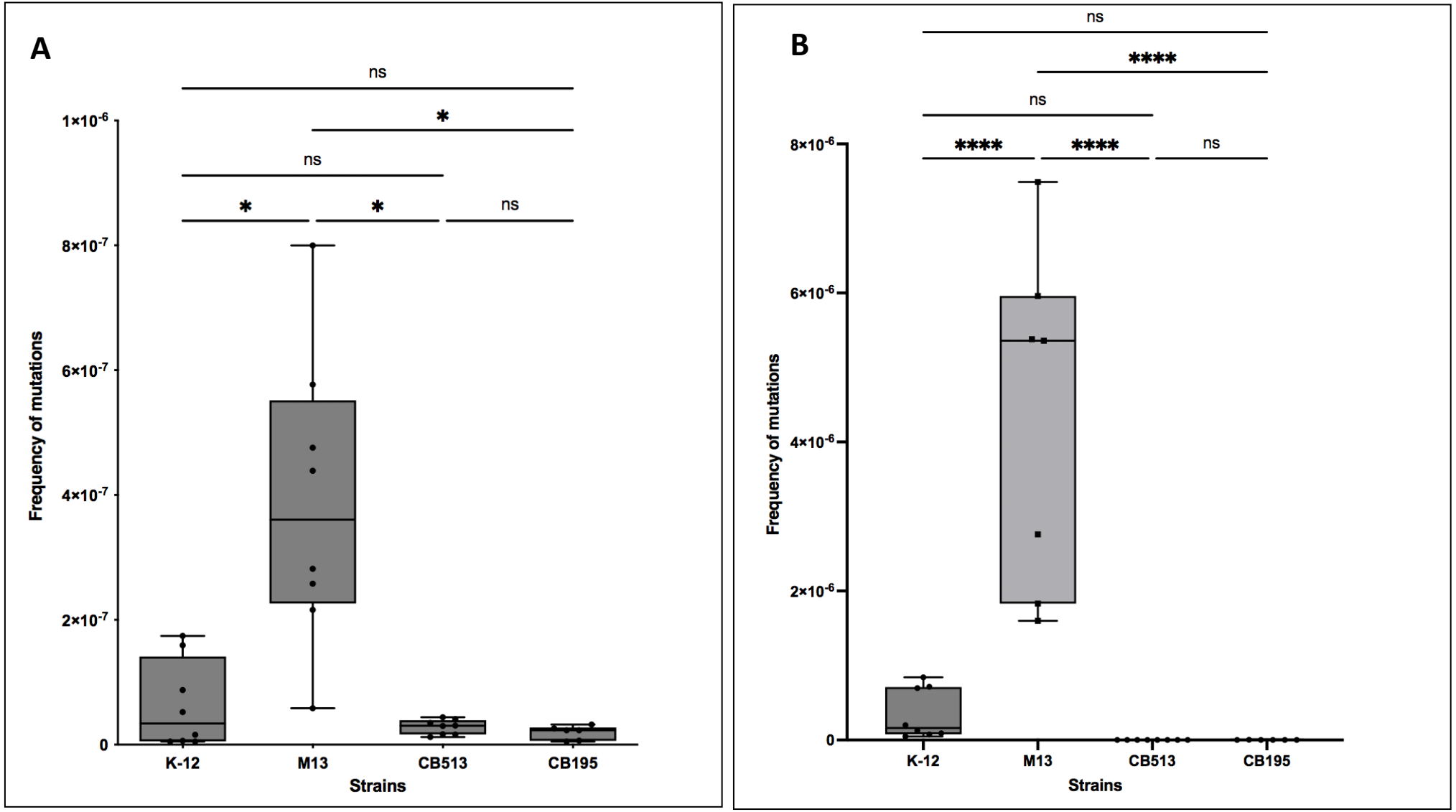

FIG S2: Boxplot representation of mutation rates of each *E. coli* donor strains (CB513 harboring p30 and CB195 harboring p46). (A) Frequency of rifampicin resistance acquisition. (B) Frequency of fosfomycin resistance acquisition. For each box, the central mark indicates the median, and the bottom and top edges of the box indicate the 25th and 75th percentiles, respectively. Each point corresponds to one measurement per clone. *E. coli* M13 and K-12 MG1655 are mutator (*mutS*-deleted) and non mutator controls, respectively. Asterisks indicate significant differences (*, $P \leq 0.05$; ****, $P \leq 0.0001$), ns = not significant.

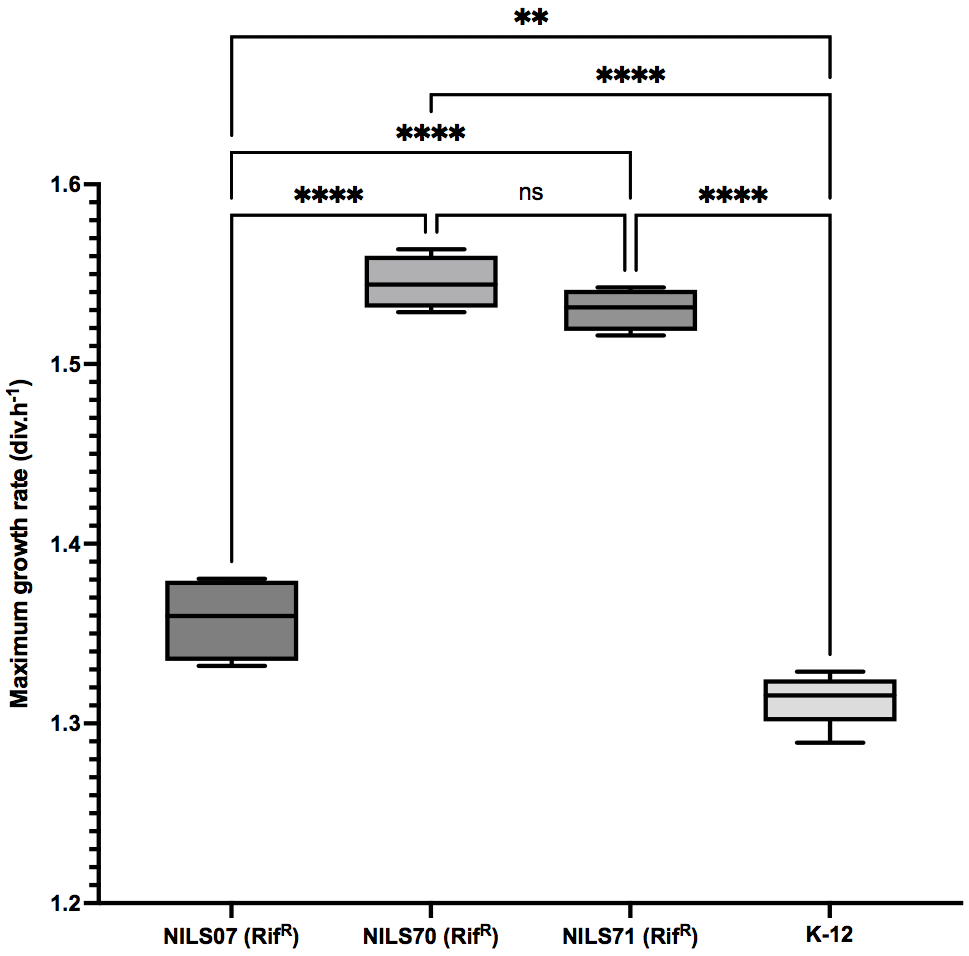

FIG S3: Box plot representation of the maximum growth rates (MGRs) of each recipient strains used in the study : NILS07, NILS70, NILS71, and K-12 MG1655. For each box, the central mark indicates the median, and the bottom and top edges of the box indicate the 25th and 75th percentiles, respectively. Asteriks indicate significant differences (**, $P \leq 0.01$; ****, $P \leq 0.0001$); ns, not significant.

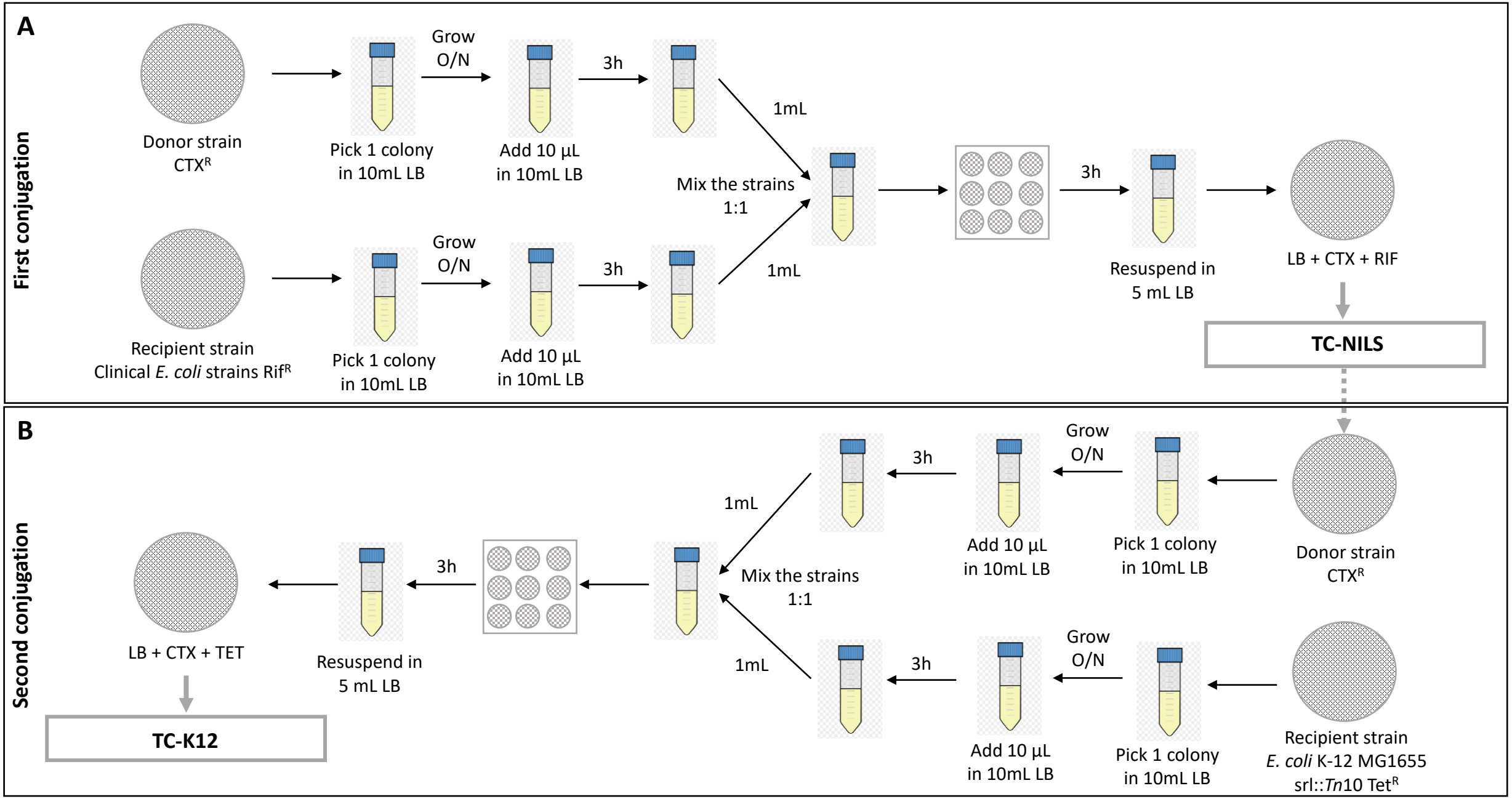

FIG S4: Design of the experimental conjugation assay. (A) First conjugation of 3 ESBL-encoding plasmids (p30 from CB513 donor strain, and p46 or p46^{r} from ancestral CB195 donor strain) in 3 *E. coli* clinical strains (NILS07, NILS70, and NILS71) resistant to rifampicin (Rif^{R}). (B) Second conjugation of 6 TC-NILS (harboring p46^{r} or p46^{nr} plasmids, with or without IncR backbone/aminoglycosides deletion) obtained from conjugation A in K-12 MG1655 srl::*Tn*10 strain, resistant to tetracyclin (Tet^{R}). CTX = cefotaxime, RIF = rifampicin, TET = tetracycline.

TAB S1: Main phenotypic and genotypic characteristics of the *E. coli* isolates used in the study

	Isolate	Origin	Phylogroup	Serotype	MLST type[a]	Plasmid replicons[b]	Plasmid	Antimicrobial resistance genes[c]	Phenotypic resistance[d]											
									CTX	ETP	GEN	AMK	TMP	SXT	NAL	CIP	TET	STR	CHL	RIF
Recipients	**NILS07**	Feces	A	O105:H6	ST10	IncB/O/K/Z_1 Col156_1, ColRNAI_1		ND	S	S	S	S	S	S	S	S	S	S	S	S
	NILS70	Urine	B2	O4:H5	ST12	ColRNAI_1		ND	S	S	S	S	S	S	S	S	S	S	S	S
	NILS71	Urine	B2	O2:H1	ST1154	ND		ND	S	S	S	S	S	S	S	S	S	S	S	S
Donors	**CB513**	Blood	F	O1:H6	ST648	IncA/C2_1 ColRNAI_1, Col8282_1, Col(BS512)_1, Col(MG828)_1	p30	*bla* $_{TEM-1B}$, *bla* $_{CTX-M-14}$, *aph(3'')-Ib, aph(6)-Id, sul2, erm(42)*	R	S	S	S	S	S	S	S	S	R	S	S
	CB195	Feces	A	O15:H38	ST1303	IncA/C2_1 IncR_1	p46	*bla* $_{CTX-M-15}$, *dfrA5, sul1, sul2, aac(3)-IId, aph(3'')-Ib, aph(6)-Id, ere(A)*	R	S	R	S	R	R	S	S	S	R	S	S
						IncA/C2_1	^{S}p46^{r}	*bla* $_{CTX-M-15}$, *dfrA5, sul1, ere(A)*	R	S	S	S	R	R	S	S	S	S	S	S

[a], according to the Warwick multilocus sequence typing (MLST) scheme; [b], PlasmidFinder; [c], ResFinder; [d], R = resistant, S = sensitive. CTX = cefotaxime, ETP = ertapenem, GEN = gentamicin, AMK = amikacin, TMP = trimethoprim, SXT = sulfonamides + trimethoprim, NAL = nalidixic acid, CIP = ciprofloxacin, TET = tetracycline, STR = streptomycin, CHL = chloramphenicol, RIF = rifampicin. ND = Not detected. [S], p46 plasmid which spontaneously exhibited rearrangements into the MDR-encoding region and selected from the ancestral donor strain CB195 (designated p46^{r})

TAB S2: Main phenotypic and genotypic characteristics of the *E. coli* transconjugants obtained from the first conjugation assay

NILS-transconjugant (TC-NILS)	Donor	Recipient	Phylogroup	Serotype	MLST type[a]	Plasmid replicons expected	Plasmid replicons obtained[b]	Antimicrobial resistance genes[c]	Phenotypic resistance[d]												IncR backbone/aminoglycosides rearrrangements[e] (size in bp)
									CTX	ETP	GEN	AMK	TMP	SXT	NAL	CIP	TET	STR	CHL	RIF	
TC563	**CB195** ([$]p46[$] plasmid)	**NILS07**	A	O105:H6	ST10	IncA/C2_1 ; IncB/O/K/Z_1 Col156_1 ; ColRNAI_1	IncA/C2_1 ; IncB/O/K/Z_1 Col156_1 ; ColRNAI_1	*blaCTX-M-15, dfrA5_1, sul1_5*	R	S	S	S	R	R	S	S	S	S	S	R	None
TC16		**NILS70**	B2	O4:H5	ST12	IncA/C2_1 ColRNAI_1	IncA/C2_1	*bla $_{CTX-M-15}$, dfrA5_1, sul1_2*	R	S	S	S	R	R	S	S	S	S	S	R	None
TC22a		**NILS71**	B2	O2:H1	ST1154	IncA/C2_1	IncA/C2_1	*bla $_{CTX-M-15}$, dfrA5_1, sul1_2*	R	S	S	S	R	R	S	S	S	S	S	R	None
TC568	**CB195** (p46 plasmid)	**NILS07**	A	O105:H6	ST10	IncA/C2_1 ; IncB/O/K/Z_1 Col156_1 ; ColRNAI_1	IncA/C2_1 ; IncB/O/K/Z_1 Col156_1 ; ColRNAI_1	*bla $_{CTX-M-15}$, aac(3)-IId_1, dfrA5_1, sul1_5, sul2_3, aph(3'')-Ib_5, aph(6)-Id_1*	R	S	R	S	R	R	S	S	S	R	S	R	Yes (84,517)
TC569			A	O105:H6	ST10	IncA/C2_1 ; IncR_1 ; IncB/O/K/Z_1 Col156_1 ; ColRNAI_1	IncA/C2_1 ; IncR_1 ; IncB/O/K/Z_1 Col156_1 ; ColRNAI_1	*bla $_{CTX-M-15}$, aac(3)-IId_1, sul2_3, aph(3'')-Ib_5, aph(6)-Id_1*	R	S	R	S	S	S	S	S	S	R	S	R	None
TC570			A	O105:H6	ST10	IncA/C2_1 ; IncR_1 ; IncB/O/K/Z_1 Col156_1 ; ColRNAI_1	IncA/C2_1 ; IncR_1 ; IncB/O/K/Z_1 Col156_1 ; ColRNAI_1	*bla $_{CTX-M-15}$, aac(3)-IId_1, dfrA5_1, sul1_5, sul2_3, aph(3'')-Ib_5, aph(6)-Id_1*	R	S	R	S	R	R	S	S	S	R	S	R	None
TC574			A	O105:H6	ST10	IncA/C2_1 ; IncB/O/K/Z_1 Col156_1 ; ColRNAI_1	IncA/C2_1 ; IncB/O/K/Z_1 Col156_1 ; ColRNAI_1	*bla $_{CTX-M-15}$, aac(3)-IId_1, sul2_3, aph(3'')-Ib_5, aph(6)-Id_1*	R	S	R	S	S	S	S	S	S	R	S	R	Yes (105,846)
TC575			A	O105:H6	ST10	IncA/C2_1 ; IncR_1 ; IncB/O/K/Z_1 Col156_1 ; ColRNAI_1	IncA/C2_1 ; IncR_1 ; IncB/O/K/Z_1 Col156_1 ; ColRNAI_1	*bla $_{CTX-M-15}$, dfrA5_1, sul1_5*	R	S	S	S	R	R	S	S	S	S	S	R	Yes (13,345)
TC577			A	O105:H6	ST10	IncA/C2_1 ; IncB/O/K/Z_1 Col156_1 ; ColRNAI_1	IncA/C2_1 ; IncB/O/K/Z_1 Col156_1 ; ColRNAI_1	*bla $_{CTX-M-15}$, dfrA5_1, sul1_5*	R	S	S	S	R	R	S	S	S	S	S	R	Yes (13,345 and 41,697)
TC513		**NILS70**	B2	O4:H5	ST12	IncA/C2_1 ; IncR_1 ColRNAI_1	IncA/C2_1 ; IncR_1	*bla $_{CTX-M-15}$, aac(3)-IId_1, sul2_3, aph(3'')-Ib_5, aph(6)-Id_1*	R	S	R	S	S	S	S	S	S	R	S	R	None
TC514			B2	O4:H5	ST12	IncA/C2_1 ColRNAI_1	IncA/C2_1	*bla $_{CTX-M-15}$, dfrA5_1, sul1_5*	R	S	S	S	R	R	S	S	S	S	S	R	Yes (13,345 and 48,775)
TC521			B2	O4:H5	ST12	IncA/C2_1 ColRNAI_1	IncA/C2_1	*bla $_{CTX-M-15}$, dfrA5_1, sul1_5, sul2_3, aph(3'')-Ib_5, aph(6)-Id_1*	R	S	S	S	R	R	S	S	S	R	S	R	Yes (8,231 and 44,739)
TC553			B2	O4:H5	ST12	IncA/C2_1 ColRNAI_1	IncA/C2_1	*bla $_{CTX-M-15}$, aac(3)-IId_1, sul2_3, aph(3'')-Ib_5, aph(6)-Id_1*	R	S	R	S	S	S	S	S	S	R	S	R	Yes (105,846)
TC539		**NILS71**	B2	O2:H1	ST1154	IncA/C2_1	IncA/C2_1	*bla $_{CTX-M-15}$, aac(3)-IId_1, sul2_3, aph(3'')-Ib_5, aph(6)-Id_1*	R	S	R	S	S	S	S	S	S	R	S	R	Yes (105,846)
TC544			B2	O2:H1	ST1154	IncA/C2_1	IncA/C2_1	*bla $_{CTX-M-15}$, dfrA5_1, sul1_5, sul2_3, aph(3'')-Ib_5, aph(6)-Id_1*	R	S	S	S	R	R	S	S	S	R	S	R	Yes (8,231 and 74,459)
TC545			B2	O2:H1	ST1154	IncA/C2_1 ; IncR_1	IncA/C2_1 ; IncR_1	*bla $_{CTX-M-15}$, dfrA5_1, sul1_5, sul2_3, aph(3'')-Ib_5, aph(6)-Id_1*	R	S	S	S	R	R	S	S	S	R	S	R	Yes (8,231)
TC549			B2	O2:H1	ST1154	IncA/C2_1 ; IncR_1	IncA/C2_1 ; IncR_1	*bla $_{CTX-M-15}$, aac(3)-IId_1, dfrA5_1, sul1_5, sul2_3, aph(3'')-Ib_5, aph(6)-Id_1*	R	S	R	S	R	R	S	S	S	R	S	R	None
TC608	**CB513** (p30 plasmid)	**NILS07**	A	O105:H6	ST10	IncA/C2_1 ; IncB/O/K/Z_1 ColRNAI_1 ; Col8282_1 ; Col(BS512)_1 ; Col(MG828)_1 ; Col156_1	IncA/C2_1 ColRNAI_1 ; Col156_1	*blaTEM-1B_1, blaCTX-M-14, sul2_2, aph(3'')-Ib_5, aph(6)-Id_1*	R	S	S	S	S	S	S	S	S	R	S	R	NA
TC48		**NILS70**	B2	O4:H5	ST12	IncA/C2_1 ColRNAI_1 ; Col8282_1 ; Col(BS512)_1 ; Col(MG828)_1	IncA/C2_1	*bla $_{TEM-1B_1}$, bla $_{CTX-M-14}$, sul2_2, aph(3'')-Ib_5, aph(6)-Id_1*	R	S	S	S	S	S	S	S	S	R	S	R	NA
TC53		**NILS71**	B2	O2:H1	ST1154	IncA/C2_1 ColRNAI_1 ; Col8282_1 ; Col(BS512)_1 ; Col(MG828)_1	IncA/C2_1	*bla $_{TEM-1B_1}$, bla $_{CTX-M-14}$, sul2_2, aph(3'')-Ib_5, aph(6)-Id_1*	R	S	S	S	S	S	S	S	S	R	S	R	NA

[$], deletion into MDR-encoding region with the lost of the *aacC2-aph-sul2* cassette (13,345 bp), and of IncR backbone and its flanking regions (48,745 bp) compared to p46 and selected from the ancestral donor strain CB195; [a], according to the Warwick multilocus sequence typing (MLST) scheme; [b], PlasmidFinder; [c], ResFinder; [d], R = resistant, S = sensitive. CTX = cefotaxime, ETP = ertapenem, GEN = gentamicin, AMK = amikacin, TMP = trimethoprim, SXT = sulfonamides + trimethoprim, NAL = nalidixic acid, CIP = ciprofloxacin, TET = tetracycline, STR = streptomycin, CHL = chloramphenicol, RIF = rifampicin; [e], One or two deletions occurring between the transconjugants genomes and their reference plasmids for IncR plasmid backbone and aminoglycosides cassette (assignated using the open-source Breseq pipeline), NA = not applicable.

TAB S3: Maximum growth rates (MGRs) measured after the first conjugation assay

Strain	Recipient	Plasmid	Experiment 1	Experiment 2	Experiment 3	Experiment 4	Mean MGR (div/h)
			MGR (div/sec)				
NILS07 (Rif^R)			0,000365033 0,000381947 0,000372393	0,00037965 0,000379741 0,000387669	0,000360077 0,000371962 0,000378019	0,000387442 0,000384135 0,000378828	**1,358**
TC608	NILS07	p30	0,000365774 0,000343035 0,000354034	0,000358837 0,000346182 0,000343671	0,000354873 0,000337853 0,000349947	0,000344544 0,000345578 0,000350133	**1,258**
TC570		p46^{nr}	0,000354781 0,000349579 0,000352429	0,000356067 0,000338161 0,000357849	0,000333339 0,00034736 0,000343875	0,000345594 0,000345953 0,000343902	**1,251**
TC574		p46^{r-1}	0,000347887 0,00032587 0,000341705	0,000348305 0,000339883 0,000338165	0,000344248 0,000323397 0,000346754	0,000341282 0,000330081 0,000340501	**1,220**
TC575		p46^{r-2}	0,000354981 0,000353624 0,000360202	0,000348509 0,000357728 0,000349205	0,000346891 0,000358469 0,000350608	0,000330983 0,000340257 0,000317117	**1,251**
TC577		p46^{r-3}	0,000352309 0,000346562 0,000343955	0,000345961 0,000346199 0,000344254	0,000353997 0,000361477 0,000353134	0,000342999 0,000340078 0,00034354	**1,252**
NILS70 (Rif^R)			0,000432569 0,000428515 0,000412987	0,000428953 0,000434887 0,000427284	0,000425387 0,000440031 0,000437837	0,000431642 0,000434662 0,000416359	**1,545**
TR48	NILS70	p30	0,000408236 0,000422165 0,000413658	0,000425045 0,000413648 0,000428249	0,000436857 0,000430412 0,000418882	0,000414045 0,000420175 0,000417557	**1,515**
TC513		p46^{nr}	0,000399023 0,000412323 0,000406985	0,000421964 0,000430255 0,000419835	0,000430722 0,000420953 0,000425594	0,000422092 0,000410845 0,000404173	**1,501**
TC553		p46^{r-1}	0,000412063 0,000407518 0,000408469	0,000425659 0,000427023 0,0004151	0,000416838 0,000420624 0,000413366	0,000411787 0,000406624 0,000404695	**1,491**
TC521		p46^{r-2}	0,000416584 0,000415271 0,000421117	0,000412377 0,000428445 0,000428387	0,000430858 0,000424699 0,00042869	0,000418937 0,000423289 0,000405844	**1,516**
NILS71 (Rif^R)			0,00042478 0,00041603 0,000430903	0,000413697 0,000434711 0,000414861	0,000434031 0,000424766 0,000426765	0,000430459 0,000424702 0,000425622	**1,530**
TR53	NILS71	p30	0,000396812 0,000393968 0,000385609	0,000376195 0,000382984 0,00037884	0,000380458 0,000387633 0,000388014	0,000387937 0,000381173 0,000383028	**1,387**
TC549		p46^{nr}	0,000396468 0,000361589 0,000384516	0,000368859 0,000405903 0,000391931	0,00037569 0,00040154 0,000369796	0,000374687 0,000401944 0,000393969	**1,388**
TC539		p46^{r-1}	- - -	0,000382166 0,00036934 0,00037205	0,000368249 0,000374345 0,000372872	0,000366525 0,000354232 0,000360358	**1,328**
TC544		p46^{r-2}	0,000399979 0,000387716 0,000389831	0,00038641 0,000381409 0,000376553	0,00038482 0,000386372 0,000385143	0,000386563 0,000384923 0,000373232	**1,387**
TC545		p46^{r-3}	0,000382058 0,000404997 0,000376799	0,000365668 0,000392805 0,000354509	0,000374536 0,000373897 0,000388245	0,000387975 0,000380643 0,000385315	**1,370**

Rif^R: resistant to rifampicin

TAB S4: Main phenotypic and genotypic characteristics of the *E. coli* transconjugants obtained from the second conjugation assay into K-12 MG1655 srl::*Tn* 10

K12-transconjugant (TC-K12)	Donor	Chromosomal background	Plasmid	Recipient	Name in text	IncC replicon[a]	IncR replicon[b]	Phenotypic resistance[c]												Maximum growth rates (MGR, div/sec)			Mean MGR (div/h)
								CTX	ETP	GEN	AMK	TMP	SXT	NAL	CIP	TET	STR	CHL	RIF	Replicate 1	Replicate 2	Replicate 3	
TC613	TC539	NILS71	$p46^{r-1}$	K-12 MG1655 srl::Tn10 (phylogroup A)	$K12_{71}$-$p46^{r-1}$	ND	ND	R	S	R	S	S	S	S	S	R	R	S	S	0,000346822	0,000350019	0,00034486	1,255
TC614						ND	ND	R	S	R	S	S	S	S	S	R	R	S	S	0,000350732	0,000351308	0,000350897	
TC615						ND	ND	R	S	R	S	S	S	S	S	R	R	S	S	0,000356747	0,000355229	0,000355869	
TC616						ND	ND	R	S	R	S	S	S	S	S	R	R	S	S	0,0003444	0,000345652	0,000348302	
TC617						ND	ND	R	S	R	S	S	S	S	S	R	R	S	S	0,000352112	0,000342328	0,000333659	
TC618	TC544	NILS71	$p46^{r-2}$		$K12_{71}$-$p46^{r-2}$	ND	ND	R	S	S	S	R	R	S	S	R	R	S	S	0,000351572	0,000356148	0,000363499	1,283
TC619						ND	ND	R	S	S	S	R	R	S	S	R	R	S	S	0,000357254	0,000352109	0,000357885	
TC620						ND	ND	R	S	S	S	R	R	S	S	R	R	S	S	0,000356382	0,000359914	0,000362632	
TC621						ND	ND	R	S	S	S	R	R	S	S	R	R	S	S	0,000357916	0,000350788	0,000349774	
TC622						ND	ND	R	S	S	S	R	R	S	S	R	R	S	S	0,000356484	0,000359422	0,000355751	
TC623	TC553	NILS70	$p46^{r-1}$		$K12_{70}$-$p46^{r-1}$	ND	ND	R	S	R	S	S	S	S	S	R	R	S	S	0,00034566	0,000349289	0,000339984	1,264
TC624						ND	ND	R	S	R	S	S	S	S	S	R	R	S	S	0,000353556	0,000351592	0,000353402	
TC625						ND	ND	R	S	R	S	S	S	S	S	R	R	S	S	0,000356882	0,000356698	0,000358244	
TC626						ND	ND	R	S	R	S	S	S	S	S	R	R	S	S	0,000348353	0,000349053	0,000346435	
TC627						ND	ND	R	S	R	S	S	S	S	S	R	R	S	S	0,000349477	0,000354914	0,00035233	
TC628	TC574	NILS07	$p46^{r-1}$		$K12_{07}$-$p46^{r-1}$	ND	ND	R	S	R	S	S	S	S	S	R	R	S	S	0,000357382	0,000355814	0,000357427	1,264
TC629						ND	ND	R	S	R	S	S	S	S	S	R	R	S	S	0,000352452	0,000353879	0,000354907	
TC630						ND	ND	R	S	R	S	S	S	S	S	R	R	S	S	0,000349975	0,000355857	0,000352014	
TC631						ND	ND	R	S	R	S	S	S	S	S	R	R	S	S	0,000345459	0,000341191	0,000350012	
TC632						ND	ND	R	S	R	S	S	S	S	S	R	R	S	S	0,000345875	0,000347085	0,00034759	
TC643	TC570	NILS07	$p46^{nr}$		$K12_{07}$-$p46^{nr}$	+	+	R	S	R	S	S	S	S	S	R	R	S	S				1,238
TC644						+	+	R	S	R	S	S	S	S	S	R	R	S	S				
TC645						+	+	R	S	R	S	R	R	S	S	R	R	S	S	0,000349074	0,000347742	0,000349577	
TC646						+	+	R	S	R	S	R	R	S	S	R	R	S	S	0,000344002	0,000345722	0,000339873	
TC647						+	+	R	S	R	S	R	R	S	S	R	R	S	S	0,000340222	0,000348732	0,000341582	
TC658						+	+	R	S	R	S	R	R	S	S	R	R	S	S	0,000351563	0,000350163	0,000316875	
TC659						+	+	R	S	R	S	R	R	S	S	R	R	S	S	0,000347324	0,000341935	0,00034278	
TC660						+	+	R	S	R	S	R	R	S	S	R	R	S	S				
TC661						+	0	R	S	R	S	S	S	S	S	R	R	S	S				
TC662						+	+	R	S	R	S	R	R	S	S	R	R	S	S				
TC648	TC549	NILS71	$p46^{nr}$		$K12_{71}$-$p46^{nr}$	+	+	R	S	R	S	R	R	S	S	R	R	S	S				1,262
TC649						+	+	R	S	R	S	R	R	S	S	R	R	S	S	0,00035869	0,000359751	0,000357951	
TC650						+	+	R	S	S	S	R	R	S	S	R	R	S	S				
TC651						+	+	R	S	R	S	R	R	S	S	R	R	S	S	0,000336258	0,000344869	0,000352249	
TC652						+	+	R	S	R	S	R	R	S	S	R	R	S	S	0,000349747	0,000351018	0,000350818	
TC653						+	+	R	S	R	S	R	R	S	S	R	R	S	S	0,00035032	0,000353349	0,000343356	
TC654						+	+	R	S	R	S	R	R	S	S	R	R	S	S	0,000352325	0,000354537	0,000342601	
TC655						+	+	R	S	R	S	R	R	S	S	R	R	S	S				
TC656						+	+	R	S	R	S	R	R	S	S	R	R	S	S				
TC657						+	+	R	S	R	S	R	R	S	S	R	R	S	S				

[a], *repA* (IncA/C replicase gene) PCR ; [b], *repB* (IncR replicase gene) PCR. ND = not determined, 0 = absent, + = present ; [c], R = resistant, S = sensitive. CTX = cefotaxime, ETP = ertapenem, GEN = gentamicin, AMK = amikacin, TMP = trimethoprim, SXT = sulfonamides + trimethoprim, NAL = nalidixic acid, CIP = ciprofloxacin, TET = tetracycline, STR = streptomycin, CHL = chloramphenicol, RIF = rifampicin.

TAB S5: Contrast matrix of the differences in MGRs of TC-NILS, in MGRs of TC-K12, and in conjugation frequency of p46^{r} and p46^{nr} in K-12 MG1655

		Coefficients characterizing the MGRs of TC-NILS											
		β_0	β_1	β_2	β_3	β_4	β_5	β_6	β_7	β_8	β_9	β_{10}	β_{11}
Contrast ax,i for coefficient β_i and for strain *x*	NILS$_{07}$		-0.33333	-0.33333	-0.75	0	0	0	0	0	0	0	0
	NILS$_{07}$-p30		-0.33333	-0.33333	0.25	0	0	0.66667	0	0	-0.33333	0	0
	NILS$_{07}$-p46^{nr}		-0.33333	-0.33333	0.25	0	0	-0.33333	0	0	-0.33333	0	0
	NILS$_{07}$-p46^{r}		-0.33333	-0.33333	0.25	0	0	-0.33333	0	0	0.66667	0	0
	NILS$_{70}$		0.66667	-0.33333	0	-0.75	0	0	0	0	0	0	0
	NILS$_{70}$-p30		0.66667	-0.33333	0	0.25	0	0	0.66667	0	0	-0.33333	0
	NILS$_{70}$-p46^{nr}		0.66667	-0.33333	0	0.25	0	0	-0.33333	0	0	-0.33333	0
	NILS$_{70}$-p46^{r}		0.66667	-0.33333	0	0.25	0	0	-0.33333	0	0	0.66667	0
	NILS$_{71}$		-0.33333	0.66667	0	0	-0.75	0	0	0	0	0	0
	NILS$_{71}$p30		-0.33333	0.66667	0	0	0.25	0	0	0.66667	0	0	-0.33333
	NILS$_{71}$-p46^{nr}		-0.33333	0.66667	0	0	0.25	0	0	-0.33333	0	0	-0.33333
	NILS$_{71}$-p46^{r}		-0.33333	0.66667	0	0	0.25	0	0	-0.33333	0	0	0.66667
Coefficient estimate		1.40361	0.23922	0.14047	-0.10803	-0.03875	-0.15052	0.00767	0.01325	-0.00127	-0.00956	0.00221	-0.02328
P -value		<0.0001	<0.0001	<0.0001	<0.0001	0.0098	<0.0001	0.6734	0.4674	0.9442	0.5207	0.8884	0.1251

		Coefficients characterizing the MGRs of TC-K12						
		β_0	β_1	β_2	β_3	β_4	β_5	β_6
Contrasts for coefficient βi and for strain *x*	K12		-0.28571	-0.14286	-0.42857	0	0	0
	K12$_{07}$-p46^{nr}		0.71429	-0.14286	-0.42857	-0.5	0	0
	K12$_{07}$-p46^{r-1}		0.71429	-0.14286	-0.42857	0.5	0	0
	K12$_{70}$-p46^{r-1}		-0.28571	0.85714	-0.42857	0	0	0
	K12$_{71}$-p46^{nr}		-0.28571	-0.14286	0.57143	0	-0.33333	-0.33333
	K12$_{71}$-p46^{r-1}		-0.28571	-0.14286	0.57143	0	0.66667	-0.33333
	K12$_{71}$-p46^{r-2}		-0.28571	-0.14286	0.57143	0	-0.33333	0.66667
Coefficient estimate		1.26846	-0.06252	-0.04960	-0.04666	0.02634	-0.00694	0.02153
P -value		<0.0001	<0.0001	<0.0001	<0.0001	0.0126	0.4886	0.0380

		Coefficients characterizing the conjugation frequency					
		β_0	β_1	β_2	β_3	β_4	β_5
Contrasts for coefficient βi and for strain x	K12$_{07}$-p46^{nr}		-0.16667	-0.5	-0.5	0	0
	K12$_{07}$-p46^{r-1}		-0.16667	-0.5	0.5	0	0
	K12$_{70}$-p46^{r-1}		0.83333	-0.5	0	0	0
	K12$_{71}$-p46^{nr}		-0.16667	0.5	0	-0.33333	-0.33333
	K12$_{71}$-p46^{r-1}		-0.16667	0.5	0	0.66667	-0.33333
	K12$_{71}$-p46^{r-2}		-0.16667	0.5	0	-0.33333	0.66667
Coefficient estimate		-7.36376	4.18251	-0.39361	2.40751	5.04269	4.74231
P -value		<0.0001	<0.0001	0.4012	0.0049	<0.0001	<0.0001